A review of all-vanadium redox flow battery durability: degradation mechanisms and mitigation strategies

Yuan, Xiao-Zi; Song, Chaojie; Platt, Alison; Zhao, Nana; Wang, Haijiang; Li, Hui; Fatih, Khalid; Jang, Darren

Publisher's version / Version de l'éditeur:
https://doi.org/10.1002/er.4607
International Journal of Energy Research, 43, 13, pp. 6599-6638, 2019-06-23

A review of all-vanadium redox flow battery durability: Degradation mechanisms and mitigation strategies

Xiao-Zi Yuan*, Chaojie Song*, Alison Platt, Nana Zhao, Haijiang Wang, Hui Li, Khalid Fatih, Darren Jang

Energy, Mining & Environment Research Centre, National Research Council Canada, 4250 Wesbrook Mall, Vancouver, BC, V6T 1W5, Canada

*Corresponding authors

Xiao-Zi Yuan:

Email: xiao-zi.yuan@nrc.gc.ca

Tel: 1-604-221-3000 ext.5576

Fax: 1-604-221-3001

Chaojie Song:

Email: Chaojie.song@nrc.gc.ca

Tel: 1-604-221-3000 ext.5577

Fax: 1-604-221-3001

Address: 4250 Wesbrook Mall, Vancouver, BC, V6T 1W5 Canada

Abstract

The all-vanadium redox flow battery (VRFB) is emerging as a promising technology for large scale energy storage systems due to its scalability and flexibility, high round-trip efficiency, long durability, and little environmental impact. As the degradation rate of the VRFB components is relatively low, less attention has been paid in terms of VRFB durability in comparison with studies on performance improvement and cost reduction. This paper reviews publications on performance degradation mechanisms and mitigation strategies for VRFBs in an attempt to achieve a systematic understanding of VRFB durability. Durability studies of individual VRFB components, including electrolyte, membrane, electrode, and bipolar plate are introduced. Various degradation mechanisms at both cell and component levels are examined. Following these, applicable strategies for mitigating degradation of each component are compiled. In addition, this paper summarizes various diagnostic tools to evaluate component degradation, followed by accelerated stress tests and models for aging prediction that can help reduce the duration and cost associated with real lifetime tests. Finally, future research areas on the degradation and accelerated lifetime testing for VRFBs are proposed.

Keywords: Redox flow battery; vanadium redox flow battery; durability; degradation; mitigation; diagnostic tools.

1 Introduction

Renewable resources, such as solar, wind and hydropower, are increasingly being utilized due to the depletion of fossil fuels and anthropogenic climate change. As these resources are usually unpredictable, there is an imperative need for grid-connected energy storage systems to complement and employ renewable energies [1]. Electrochemical storage systems, such as sodium sulfur batteries, lithium-ion batteries, redox flow batteries (RFBs), and lead acid batteries, offer a solution because of their flexibility, efficiency, scalability, and other appealing features. By comparing the technicalities of different energy storage devices [2], the functional capabilities and technical advantages of RFBs are well suited to meet many of the demands for large-scale grid storage.

1.1 Redox flow batteries (RFBs)

In 1971, the polarization characteristics of a redox-type fuel cell were first studied by Ashimura and Miyake using a flow-through porous carbon electrode. In 1973, the Lewis Research Center in Cleveland was established by NASA (National Aeronautics and Space Administration, U.S.A.) with the objective of researching electrically rechargeable redox flow cells [3]. They investigated the fundamental feasibility of the overall redox concept, screened candidate redox couples to achieve optimum cell performance, and conducted system analysis and modeling to estimate costs [4][5]. Since then, significant progresses on RFB chemistries, materials, and systems has been made globally.

RFBs have been gaining momentum in both research and industry due to their relatively low capital and cycle cost in comparison with other energy storage technologies [2] and their ability to efficiently store large amounts of electrical energy in a world of expanding renewable energy. The most appealing features of this technology are scalability and flexibility, independent sizing of power and energy, high round-trip efficiency, long cycling and calendar lifetimes, rapid response to load changes, reasonable capital costs, tolerance to deep discharges, and reduced environmental impact. The primary drawback of a redox system is its high volume due to the low energy density of the electrolyte, thus bearing a larger footprint.

In the traditional sense, redox systems are not batteries; they have a much greater similarity to fuel cell systems. Important RFB types include iron/chromium, bromine/polysulfide, all-vanadium, vanadium/bromine, zinc/bromine, and other configurations, each having its advantages, disadvantages, and challenges. Various types of flow batteries are summarized by Ulaganathan et al. [6] and performance characteristics are also quantitatively compared. There have been comprehensive and critical reviews of the features of this type of battery, focusing on the RFB chemistry, systematic classification, current status, recent progresses, and challenges [7][10].

A generic RFB cell consists of an anolyte (negative electrolyte), porous electrodes, a catholyte (positive electrolyte), and a separator (typically an ion-exchange membrane to separate the anolyte and catholyte solutions). The general reactions are as following [1]:

During charge:

$$\text{Anode: } B^{m+} - ye^{-} \xrightarrow{\text{charge}} B^{(m+y)+} \tag{1}$$

$$\text{Cathode: } A^{n+} + xe^{-} \xrightarrow{\text{charge}} A^{(n-x)+} \tag{2}$$

During discharge:

$$\text{Anode: } A^{(n-x)+} \xrightarrow{\text{discharge}} A^{n+} + xe^{-} \quad (3)$$

$$\text{Cathode: } B^{(m+y)+} \xrightarrow{\text{discharge}} B^{m+} - ye^{-} \quad (4)$$

The principle of a RFB cell is a pair of electrochemical reduction and oxidation reactions occurring within two liquid electrolytes containing metal ions [11]. As the cell charges, the oxidation reaction occurs on the anode and electrons are released; on the cathode, the reduction reaction occurs by receiving electrons. Electrolyte is pumped through both half-cells from external tanks while ions migrate through a polymer electrolyte membrane to maintain electric neutrality.

1.2 All-vanadium redox flow batteries (VRFBs)

Although various flow batteries have been undergoing development for the last 30 years, the all-vanadium redox battery (VRFB) has been found to be most appealing because both the anolyte and catholyte employ the same element, avoiding cross-contamination of the two half-cell electrolytes. VRFBs have become the most promising and commercially exploited RFB type for storing intermittent renewable energy [12].

A typical VRFB energy storage system is shown in Figure 1 (a), which principally consists of two key parts: the cell stacks, where chemical energy and electricity are converted in reversible processes, and the tanks, where electrolytes are stored [13]. Basically, the VRFB stack is similar to a proton exchange membrane (PEM) fuel cell stack and a single VRFB cell is similar to a PEM fuel cell, as presented in Figure 1 (b) [14].

Figure 1

In some configurations, not only the structure of a VRFB stack or a single cell, but also the membrane electrode assembly is similar to those of a PEM fuel cell. The materials used can also be similar in some cases. Ion exchange membranes used are typically Nafion® or other perfluorinated polymers; electrodes are graphite felts (GFs) or carbon felts (CFs), and bipolar plates (BPs) are graphite plates. Although researchers are recently developing new materials, these materials are not yet used in commercial VRFB systems.

In a VRFB, two simultaneous reactions occur on both sides of the membrane. The electrochemical reactions during charge and discharge are:

Positive electrode reaction:

$$VO^{2+} + H_2O - e^{-} \underset{discharge}{\overset{charge}{\rightleftharpoons}} {VO_2}^{+} + 2H^{+} \qquad E_{cathode} = 1.004V \quad (5)$$

Negative electrode reaction:

$$V^{3+} + e^{-} \underset{discharge}{\overset{charge}{\rightleftharpoons}} V^{2+} \qquad E_{anode} = -0.255V \quad (6)$$

Overall electrochemical reaction of the cell:

$$VO^{2+} + H_2O + V^{3+} \overset{charge}{\underset{discharge}{\longleftrightarrow}} VO_2{}^{+} + V^{2+} + 2H^{+} \qquad E_{cell} = 1.259V \tag{7}$$

During charging at the positive electrode, tetravalent vanadium within VO^{2+} ions (V(IV)) is oxidized to pentavalent vanadium within $VO_2{}^{+}$ ions (V(V)), while at the negative electrode trivalent ions V^{3+} (V(III)) are reduced to bivalent ions V^{2+} (V(II)). The hydrogen ions ($2H^{+}$) move through the membrane to maintain the electrical neutrality of the electrolytes. The standard open circuit voltage (OCV) of a VRFB cell is 1.26 V at 25 °C, but in reality, the cell exhibits an OCV of 1.4 V at 50% state of charge (SOC) due to proton activities, Donnan potential [15], and omission of other ionic species in the Nernst equation [16]. Considering the proton activities in the catholyte and anolyte as well as the Donnan potential, the OCV can be calculated according to the following equation [15]:

$$V_{OC} = E_0 + \frac{RT}{nF} ln[\frac{C_{V^{5+}} C_{V^{2+}} C_{H^+}^{+} (C_{H^+}^{+})^2}{C_{V^{4+}} C_{V^{3+}} C_{H^+}^{-}}] \tag{8}$$

where R is the ideal gas constant (equal to 8.314 J mol^{-1} K^{-1}), F is the Faraday constant (equal to 95,484.56 C mol^{-1}), n is the number of moles of electrons transferred in the balance equation, T is the absolute temperature (typically 298 K), $C_{H^+}^{+}$ is the proton concentration at catholyte, and $C_{H^+}^{-}$ is proton concentration at anolyte. Typically, the VRFB is operated between 20 and 80% SOC, so the actual capacity is approximately 60% of the theoretical value. There are several known side reactions that can occur during operation, most notably the evolution of H_2 at the negative electrode on charge and the evolution of oxygen at the positive electrode. Evolved H_2 and oxygen, in the form of bubbles, can impact performance by partially obstructing the flow of the electrolyte and reducing the active surface area for electrochemical reaction in the electrode. In addition, H_2 evolution has been shown to reduce mass and charge transport coefficients while evolved oxygen reduced the effective diffusion coefficients and lowered the effective ionic and thermal conductivities [17][18].

The VRFB was invented and developed by Maria Skyllas-Kazacos and her co-workers at the University of New South Wales. They successfully demonstrated the first commercial redox flow batteries employing vanadium in each half cell [19][21]. Since then, research on this technology has emerged all over the world and VRFB systems have become the most investigated RFB chemistry on a commercial scale [22].

Kear et al. [21] summarized the performance of VRFBs at the 1 kW to 1 MW scale; prototypes up to the range of MW in power and MWh in energy-storage capacity have also been demonstrated [1]. Currently, the largest scale VRFB system (200 MW/800 MWh) is being actively installed in China with plans to be fully operational in 2020 [23].

VRFBs can be used for small scale applications (detached houses, for example); however, they are more suited to be employed for large-scale energy storage. Installations are often coupled with renewable energy sources, such as photovoltaic power plants or wind parks, or utilized for peak shaving or load shifting applications. These applications require not only a long term durability, but also a steady performance output.

1.3 VRFB degradation

VRFBs have been widely studied for storing intermittent renewable energies due to the following advantages [6][24]:

- Vanadium is relatively abundant and the electrolyte solution is relatively easy to prepare;
- The capacity can be easily adjusted by varying the solution volume and monitored by measuring the open-circuit cell voltage;
- Unlike other secondary rechargeable systems, such as lead acid and lithium-ion batteries, VRFBs have very little environmental impact; the redox couple reactions do not generate any toxic gases and the batteries have a low risk of explosion;
- Both the anolyte and the catholyte can be readily recycled;
- The electrolyte acts as a secondary cooling system that allows heat to be readily extracted from the stack, which reduces the burden on thermal management systems;
- Very fast recharging rates compared with conventional batteries;
- The same reactive element and the same supporting electrolyte are used in both half-cells, limiting cross-contamination;
- The VRFB system is considered very stable, offering long calendar life and unlimited electrolyte cycle life; the overall battery life is determined by the stability of the cell stack components.

To date, most studies have been devoted to the development of VRFB materials/components in an attempt to improve performance and reduce cost. A few excellent reviews have been published summarizing progresses of the VRFB development [12][13][21][25]. Reviews at a component level on electrolytes [24][26], electrodes [27], and membranes [28][30] can also be found. In this journal specifically, only three reviews on the topic of VRFBs exist to date and all focus on general technology development.

The most important advantage of VRFBs is their durability and low-rate degradation. It is claimed that VRFBs have a cycle life over 12,000 cycles [31]. Although numerous demonstrations have further commercialized the VRFB technology, there are still some remaining challenges that need to be addressed or overcome. The high cost of vanadium electrolyte and membranes, the high purity requirements for the vanadium oxide raw material, and the electrode corrosion during overcharging all lead to decreased cell performance and increased stack material costs [24]. Overall, the key issue is the high cost of the VRFB system, roughly $400-500 per kWh. To broadly penetrate the market, both the capital and cycle life cost of VRFBs need to be significant reduced [12]. While improving the performance of the VRFB cell/stack by exploring novel materials with lower cost could be the most effective way, further boosting of cell/stack durability shouldn't be underestimated to efficiently extend the operational life span; durability of the VRFB system is the major key to its future success. In fact, the degradation of the VRFB materials and the VRFB system has attracted much less attention to date than the performance improvement and a thorough literature search shows that only a few publications are available on the degradation of a VRFB or on stability tests of electrode material. Thus, the underlying basic science of the degradation for VRFB materials/components is not yet fully understood. Also, at the time of publication, there have been no comprehensive reviews of the literature related to the VRFB degradation. As such, this paper reviews publications on performance degradation and mitigation strategies for VRFBs with a unique objective to achieve a systematic understanding of VRFB durability with a focus on degradation of commercialized materials. It should be noted that this review is focused on component and cell-level durability issues, therefore issues of system integration are not examined, although they can be critically important for system commercialization.

The structure of this paper is as follows: after an introduction and short overview of RFBs and VRFBs, durability studies of individual VRFB components, including electrolyte, membrane, electrode, and BP, are presented. Various degradation mechanisms at both cell and component levels are examined. Following these, applicable mitigation strategies for alleviating degradation of each component are emphasized. In addition, this paper summarizes accelerated stress tests for VRFBs to prevent prolonged test periods and high costs associated with real lifetime tests. To close, future research areas on the degradation and accelerated lifetime testing are proposed.

2 Degradation of VRFB components

Degradation of VRFBs can be caused by various mechanisms such as electrolyte contamination, electrode corrosion, corrosion of BPs, ion-exchange membrane breakage, and blockage of liquid pipe due to electrolyte crystallization. To predict cell degradation is challenging as the VRFB system contains several key components with each component having its own degradation mechanisms. As such, mitigation strategies to reduce component degradation could be diversified. Although experimental data on the degradation mechanisms of the VRFB system are not extensively reported, this section aims to give a systematic overview of component degradation mechanisms, mitigation strategies, as well as diagnostic tools for performance and degradation.

2.1 Electrolyte

The electrolyte is one of the most important components of VRFBs. While the size of the stack decides the power of the VRFB, the electrolyte volume determines the battery capacity. In addition, the properties of the electrolyte could significantly affect the cell performance as well as the overall battery cost [24].

2.1.1 Commonly used electrolyte

The most commonly used redox couples in a VRFB system are V(II)/V(III) and V(IV)/V(V) (Equations (5) and (6)) in the negative and positive half-cell electrolytes, respectively. Skyllas-Kazacos and co-workers conducted a series of studies to screen various supporting electrolytes, such as HCl, H_2SO_4, and $HClO_4$. The results showed that sulfuric acid offered the best combination of vanadium-ions solubility and redox-couple reversibility for VRFB applications [24]. Although the overcharge reaction in sulfuric acid would result in oxygen evolution, the produced gas is safe and environmentally acceptable. As such, H_2SO_4 has been chosen as the preferred supporting electrolyte for both the V(II)/V(III) and V(IV)/V(V) redox couples.

The capacity of a VRFB is dependent on the concentrations of the vanadium ions which, in turn, are dictated by the solubility of each of the redox couple ions V(II), V(III), V(IV) and V(V). The solubility of each ion is a function of temperature, sulfuric acid concentration, and SOC. The precipitation of V_2O_5 at elevated temperatures [32][35] and the low solubility of VSO_4, $V_2(SO_4)_3$, and $VOSO_4$ at low temperatures [36] limit the maximum vanadium ion concentration to 2 M, energy capacity to < 25 Wh kg^{-1}, and the operating temperature range to 10-40 °C [32]. This narrow operational temperature window, in particular its upper limit (40 °C), makes electrolyte temperature control necessary for practical applications.

In principle, vanadium electrolytes in a VRFB do not degrade and they shall remain the same even after the life of the VRFB energy storage system. The vanadium electrolytes recovered from an old VRFB at its end of life can theoretically be used for a new VRFB system. This is one of the advantages of the VRFB energy storage system, which makes the lifetime cost of the VRFB lower

than competitive energy storage systems. In reality, the vanadium electrolyte does degrade during operation, affecting the efficiency and performance of the VRFB. The following sections address the loss of efficiency and performance caused by electrolyte degradation or changes related to the vanadium electrolyte.

2.1.2 Electrolyte degradation mechanisms

Electrolyte degradation is associated with vanadium chemistry, which is extremely complex. The complexity of the vanadium chemistry is attributed to the large number of different species existing at different potentials and pH values, as well as multifarious side reactions and processes. These reactions and processes include: (i) hydrogen evolution at the negative electrode; (ii) the oxidation of the V(II) ions in the presence of air at the negative electrode; (iii) oxygen evolution at the positive electrode; (iv) vanadium ions transfer from one half-cell to the other; and (v) electrolyte transfer from one half-cell to the other due to pressure differential [26]. A better understanding of vanadium chemistry helps to comprehend electrolyte degradation. Major degradation mechanisms of the VRFB electrolyte include electrolyte precipitation, electrolyte impurities, and other changes related to the electrolyte.

2.1.2.1 Electrolyte precipitation

During the VRFB operation, all vanadium species (V(II) and V(III) in the anolyte and V(IV) and V(V) in the catholyte) may precipitate [33], causing potential blockages in the stacks and pumps and thus serious complications leading to component degradation that limits the energy density and capacity of the VRFB.

Electrolyte precipitation is closely related to the vanadium ion solubility and temperature stability. In other words, vanadium concentration in the VRFB electrolyte, a decisive factor for the energy density of VRFBs, is determined by the solubility and temperature stability of vanadium ions in different oxidation states and significantly influenced by the supporting electrolyte. To prevent precipitation of vanadium from potential blockages in the stacks and pumps, a maximum vanadium concentration should be employed over the operating temperature range. Skyllas-Kazacos and co-workers [24] summarized the solubility of each V(II), V(III), V(IV), and V(V) species in sulfuric acid at different temperatures and acid concentrations to help define these limits.

It has been identified that V(V) is the most unstable species among other vanadium species and most easily precipitates into crystals of V_2O_5 at a fully charged state of the VRFB cell. As a result, the V(V) chemistry and the V(V) stability have been the most studied topics for the VRFB electrolyte. Among various research groups, Skyllas-Kazacos' group has been the most active in investigating how to increase the thermal stability of V(V) at different concentrations [32][37], precipitation phenomenon of V(V) at different temperatures, solution compositions and solution SOC [33], and precipitation inhibitors for supersaturated vanadyl electrolyte V(IV) [38]. They have also studied how to optimize the electrolyte in terms of concentration, temperature, precipitation behavior, density, and viscosity [35].

Vijayakumar et al. [39] demonstrated that the V(V) species exists as a hydrated penta coordinated vanadate ion ($VO_2(H_2O)_3^+$). This molecule is stable at low temperatures but undergoes a deprotonation reaction at elevated temperatures forming the neutral $VO(OH)_3$ species; this neutral molecule then undergoes a condensation reaction to form the V_2O_5 precipitate. This thermal

precipitation reaction, reversible only by electrochemical means, is shown in Equations (9) and (10). Therefore, increasing the temperature decreases the stability of V(V) solutions.

$$(VO_2(H_2O)_3)^+ \overset{\Delta}{\rightarrow} VO(OH)_3 + H_3O^+ \quad (9)$$

$$2VO(OH)_3 \rightarrow V_2O_5 \cdot 3H_3O \downarrow \quad (10)$$

In addition to the temperature, sulfuric acid concentration also plays a key role in stabilizing the V(V) solution. It has been observed that increasing total sulfate/bisulfate concentration results in an increased stability of V(V) solution. For example, at 40 °C, the apparent V(V) concentration of a 3 M V(V) solution is merely 1.6 M in 5 M sulfate/bisulfate whereas it is 2.8 M in 6 M sulfate/bisulfate [35]. The increased stability at higher sulfuric acid concentration is due to the higher H^+ ions favoring the backward direction of Equation (9).

Although higher sulfuric acid concentration is beneficial in promoting the stability of V(V), the limitation of sulfuric acid concentration arises from the lower solubility of V(II), V(III) and V(IV) at elevated sulfuric acid concentrations. The reduced solubility of these species is due to the common ion effect because, unlike V(V) which undergoes a thermal precipitation, each of these species precipitates as vanadium sulfate salts.

Zhao et al. [40] studied the solubility and the solubility parameters of V(III) species in the anolyte at various concentrations of H_2SO_4 and different temperatures. Their results showed that dissolution of V(III) is an exothermic process and, as a result, the solubility of V(III) decreases with temperature (15-40 °C) and with prolonged exposure to lower temperatures. It was also found that a low concentration of H_2SO_4 can keep high concentration of V(III) stable for a long time. Specifically, the concentration of V(III) could reach 2.73 M with 1 M H_2SO_4 at 30 °C and could be stable for at least 100 days.

Xiao et al. [41] studied the physical properties of V(II), V(III), V(3.5), V(IV), and V(V) at sub-zero temperatures. Results showed that the low temperature precipitations could re-dissolve back into solution after being warmed to room temperature for 30 minutes, proving that the process is reversible. The same, however, does not apply to the V(V) precipitate where electrochemical means are required to re-dissolve the V_2O_5 precipitate back into solution.

The above results demonstrate that the solubility of V(II), V(III), and V(IV) decreases with decreasing temperature and increasing acid concentration while the opposite trends hold true for V(V). As a result, there has to be a balance in choosing the optimal temperature range, vanadium concentration, and sulfuric acid concentration for VRFB applications. Based on numerous studies by multiple research groups, the preferred electrolyte composition for the operating temperature range between 10 and 40 °C has been determined to be 1.6-2 M vanadium and 4-5 M total sulfate [24].

2.1.2.2 Effect of impurities

During the VRFB operation, impurities in the vanadium electrolyte may be present either from the raw material used to manufacture the electrolyte or from incompatible components within the system. Recently Cao et al. [42] published a thorough review on impurities and additives on VRFBs. The presence of impurities affects electrolyte stability, electrochemical kinetics, energy density, and overall cell performance.

Kubata et al. [43] measured the impact of Si and NH_4 on the VRFB performance. It was found that 40 ppm NH_4 in 2 M V / 2 M H_2SO_4 / 0.14 M H_3PO_4 / 4 ppm Si electrolyte distinctly slowed the flow rate into the cell stack within 5 charge–discharge cycles, indicating NH_4 had deposited on the felt electrode and partially blocked the electrolyte flow. Lower concentrations of NH_4 (18 and 20 ppm) were found to have negligible effects. The same group observed a significant increase in cell resistance with the addition of 100 ppm Si to 2 M V / 2 M H_2SO_4 / 0.14 M H_3PO_4 / 18 ppm NH_4 electrolyte, high enough to make the system inoperable. A moderate but continuing increase in resistance was also observed with 50 ppm Si while 40 ppm causes no effect. The effect of Si on resistance was more profound with 1.7 M V / 2.6 M H_2SO_4 / 0.12 M H_3PO_4 / 20 ppm NH_4 electrolyte. While 40 ppm significantly increased the resistance, 10 ppm Si resulted in a step-change increase and 4 ppm showed no effect on the resistance. Although Kubata et al. were able to show the adverse impact of Si on VRFB cell performance, they did not provide any information regarding the mechanism of the degradation or whether the presence of NH_4 had an impact on the Si effects.

As part of his Master's Thesis, Burch [44] was able to supplement the work done by Kubata et al. Through scanning electron microscope/energy-dispersive X-ray spectroscopy (SEM/EDS) analysis, Burch confirmed that Si accumulated on VRFB electrodes and that the blockage was a physical phenomenon, not electrochemical; in this case, the electrodes acted as a filter, permanently removing particulates from the electrolyte. Burch, however, did not observe an increase in cell resistance at an estimated 14 ppm level of Si in 1 M V / 5 M H_2SO_4 and concluded that the additional NH_4 in Kubata's work had magnified the effects. Burch also examined electrolytes prepared with $VOSO_4$ of increasing purity from various suppliers; each included the analyzed impurities provided by the suppliers for comparison. Significant variation in performance was observed. Burch found that the least pure solution yielded the lowest performance while the most pure solution produced the highest performance. He also found that the blockage of electrode pores accounted for the performance variation of the three suppliers tested. In addition, the largest variation observed was in the mass transport area, demonstrating that impurities were impacting the reactant transport through the electrodes, reducing the operational window and capacity of the battery. To prevent the effect of impurities, he proved that filtration of low-purity electrolyte was able to remove the insoluble impurities, and thus improve current densities.

Some metals such as Ag, Cr, Cu, Fe, Mn, Mo, Ni, and Sn are known to catalyze the evolution of hydrogen which may impact the performance of VRFBs [24]. In particular, Ag, Cu, Ni, and Sn are certain to deposit on the negative electrode during charging as their standard reduction potentials are less negative than V(II)/V(III). Other impurities may also deposit within the pores of the membrane; however, there is a lack of a systematic study in the public knowledge and future research is welcomed.

Recently, Park et al. [45] performed a systematic study on the influence of impurities on VRFBs. Influence of alkali ions and transition metal ions were investigated. It was found that most of the ions affect the V(II)/V(III) redox reaction rather than V(IV)/V(V). Of the alkali ions, Li^+ decreased the VRFB performance the most, resulting in irreversibility of the anolyte redox reaction. Transition metal ions Cr^{3+} and Ni^{2+} also negatively affected the VRFB performance by significantly slowing the reaction kinetics. The effects of all tested metals are summarized in Table 1.

Table 1

Although the collective research studying VRFB electrolyte impurities has been steady over the past decade, there is still substantial work to be done. In-depth analysis of a broad range of impurities at varying concentrations is required; such research should include identification of degradation mechanisms as well as interactive effects between impurities.

2.1.2.3 Impacts caused by other changes related to the electrolyte

In addition to electrolyte precipitation and electrolyte impurity, the crossover of electrolyte is another form of electrolyte degradation in VRFBs. The crossover of electrolyte not only lowers the energy efficiency but also causes the imbalance of the vanadium species across the membrane. The amount of vanadium species that cross through the membrane depends on the type of membrane employed. As the crossover of electrolyte is closely related to membrane degradation, this will be discussed in details in membrane degradation.

During VRFB operation there may be other changes in the supporting electrolytes, for example, evaporation of solvent (water). These changes may also cause electrolyte degradation although the changes are expected to be very slow. So far, there are no studies reported on the impacts of these changes in the electrolyte, therefore, an opportunity exists for future work in the research community.

2.1.3 Diagnostic tools for electrolyte degradation

2.1.3.1 Visual observation

A simple but crude method of diagnosing electrolyte degradation is via visual observation. This is possible due to the unique vanadium chemistry: distinct color changes of vanadium ions at different valent states. In aqueous solution, the solution color changes when vanadium ions undergo oxidation:

V(II) (violet) → V(III) (green) → V(IV) (blue) → V(V) (yellow)

Within the same valence state, the color of vanadium solutions may also change. For example, the color of V(V) solutions in H_2SO_4 alters with the H_2SO_4 concentration: from green in 4 M H_2SO_4 to yellow in 4-5 M H_2SO_4, and further to yellow/red in 7-8 M H_2SO_4 [46]. This color change indicates that there exists a variety of V(V) complex species at different concentrations of V(V) and H_2SO_4, possibly due to changes in the coordination geometry of the V(V) complex [24].

This unique feature not only allows visual observation of electrolyte degradation, but also estimation of the SOC of the solutions. The effectiveness, however, is limited to laboratory-scale applications where piping is usually transparent with small diameter and an operator is typically on-site.

2.1.3.2 Electrolyte property measurement

In practical applications, the properties of the vanadium electrolyte will impact the characteristics, behavior, and performance of the vanadium battery, reflecting the degradation of the electrolyte. Important properties of the VRFB electrolyte include conductivity, density, and viscosity. These properties vary with supporting electrolyte composition, SOC, and temperature.

The conductivity of the electrolyte is an important parameter for all electrochemical cells as it contributes to the cell's ohmic resistance which, in turn, affects the energy efficiency. The conductivities of the vanadium electrolytes have been measured as a function of vanadium and sulfuric acid concentrations [46][47]. In general, as the vanadium concentration increases for each of the vanadium ions, the electrolyte conductivity decreases due to the shift in the acid dissociation equilibria.

Another important property of the electrolyte is density. Mousa [48] measured the density of a series of V(III) sulfate solutions at different temperatures . The results show that a second-order model fits with respect to both the acid and V(III) sulfate concentration whereas a first order model fits with respect to temperature.

The viscosity of the VRFB electrolyte also plays an important role at both the cell and system level. Mousa [48] measured the viscosity of V(III) sulfate solutions (0-1.5 M V(III) sulfate and 1-2 M sulfuric acid) at temperatures between 15 and 40 °C. As expected, viscosity of the solution decreases with increasing temperature. This is explained by the increase in the kinetic energy of the species in solution and less solute–solvent and solute–solute interactions, leading to a decrease in resistance/friction against the flow of the solution at a high temperature. A decrease in viscosity is beneficial in terms of pumping efficiency, resulting in lower parasitic losses for the energy storage system. Recently, Li et al. established a promising method of using viscosity to determine the real-time SOC of an operating VRFB, simply by measuring pressure, flow, and temperature [49].

2.1.3.3 Quantitative/qualitative analysis of vanadium ions solutions

As aforementioned, the chemistry of vanadium electrolytes is quite complex, especially in the V(IV) and V(V) oxidation states. Considerable research has been carried out to gain a molecular-scale understanding of vanadium chemistries in solutions of vanadium/sulfuric acid. As such, quantitative measurements of vanadium ions at different oxidation states and their concentrations are important in understanding vanadium chemistries in operating VRFBs. Spectroscopic tools such as Ultraviolet (UV) spectroscopy, nuclear magnetic resonance (NMR), and Raman spectroscopy have been evaluated for quantitative and qualitative analyses of VRFB electrolytes.

Due to the distinctive color differences, UV visible (UV/Vis) spectroscopy can be used for analyzing each of the vanadium ions in sulfuric acid. Brooker et al. [50] described the method in detail to generate quantitative concentrations of different vanadium ions in a VRFB. In terms of the ion concentration values, the UV/Vis method has proven to be more reliable than either the electrode voltage or the integrated current with respect to time. Typical UV spectra for the vanadium electrolytes can be found in Choi et al.'s review paper [26]. UV has also shown potential to be used for monitoring the SOC. For the anolyte, a linear relationship between absorbance and the SOC was found over the SOC range of 5-100% [51]. The relationship between the SOC and absorbance for the catholyte, however, is non-linear due to interference between V(IV) and V(V) and the formation of complex ions; therefore, the absorbance spectrum of catholyte is much more challenging. Further research is necessary to understand the simultaneous effects of SOC, complex formations, and acidity.

NMR spectroscopy has also proven to be a useful tool for studying the vanadium chemistry in sulfuric acid solutions. ^{1}H, ^{17}O, and ^{51}V NMR spectroscopy have been used to investigate the structure and dynamics of the molecules in VRFB electrolytes. Owing to its diamagnetism, the

only oxidation state of vanadium ions active in ^{51}V NMR is V(V). The other oxidation states are paramagnetic, resulting in a significant broadening of the vanadium NMR lines. Vijayakumar et al. [39] applied ^{17}O and ^{51}V NMR spectroscopy and density functional theory-based computational modeling to investigate the solubility of V(V) electrolyte solution. The same research group also conducted ^{1}H and ^{17}O NMR analyses for a V(IV) electrolyte with varying vanadium concentrations and temperatures [52].

Raman spectroscopy has shown to be valuable in monitoring changes in the V–O bond. Several studies on the chemistry of vanadium compounds have been carried out by using this method. Griffith and co-workers [53][55] conducted a thorough investigation of the chemical composition of 2.0 M V(V) solutions over the entire pH range (1-14). Madic and co-workers [56] investigated the chemical composition of V(V) solutions in highly concentrated sulfuric acid and perchloric acid solutions. Kausar and co-workers [37] studied the chemistry of supersaturated solutions of V(V) and V(IV) in highly concentrated sulfuric acid solutions. The Raman spectra of mixed solutions of V(IV) and V(V) ions was also investigated by Kausar et al. For V(V) electrolyte, the V–O–S and V–O–V peaks increased with vanadium concentration, in good agreement with the high temperature instability at high vanadium concentrations for the V(V) electrolyte [37].

Other methods that can also be used for the quantitative analysis of total vanadium concentrations include atomic absorption spectroscopy and inductively coupled plasma analysis; however, significant errors can arise involving matrix effects when using these techniques [24].

2.1.4 Mitigation strategies for electrolyte degradation

2.1.4.1 Precipitation inhibitors

Based on the electrolyte degradation mechanisms, one of the most important mitigation strategies would be to prevent the precipitation of the vanadium ions by controlling the electrolyte concentration. For example, the solubility of the V(II), V(III), V(IV), and V(V) ions limit the practical concentration of the VRFB electrolyte to 1.6-1.8 M for an operating temperature range of 10-40 °C. To prevent thermal precipitation, a total sulfate concentration closer to 5 M is recommended to stabilize V(V) for warm climates. A lower total sulfate concentration closer to 4 M is preferred to minimize the risk of precipitation of V(II) and V(III) ions for cold climates.

For supersaturated high concentration solutions, precipitation inhibitors could be used as an important mitigation strategy in order to stabilize vanadium ions and prevent their precipitation during charge–discharge cycling of the VRFB. It is important to note that any additives or complexing agents used to enhance solubility and thermal stability must be compatible with both half-cell reactions to prevent cross-contamination through the membrane. Skyllas-Kazacos and co-workers were the first to prove that precipitation inhibitors could be successful [36][57]. Numerous research groups have studied a wide range of organic and inorganic additives as precipitation inhibitors for supersaturated V(II), V(III), V(IV), and V(V) electrolytes, although most organic additives were unstable in the presence of highly oxidizing V(V) species [24]. Ammonium phosphate, ammonium sulfate, Flocon 100, phosphoric acid, potassium phosphate, potassium sulfate, sodium pentapolyphosphate, sodium hexametaphosphate, sodium pyrophosphate dibasic, and urea have all exhibited promising results [38][58][62].

Cell cycling experiments confirmed that ammonium phosphate could dramatically extend cell operation of a 2 M solution of vanadium without precipitation over more than 250 cycles at 5 °C,

compared with less than 15 cycles for a solution without additives [58]. Skyllas-Kazacos and co-workers [38] found that K_2SO_4, $(NaPO_3)_6$ and CH_4N_2O (urea) additives could be effectively used to inhibit V(IV) precipitation in a supersaturated 4 M $VOSO_4$ / 3 M H_2SO_4 solution at 4 °C.

The use of H_3PO_4 to reduce V(V) precipitation at higher temperatures was also well recognized. Roe et al. [59] found adding 1 wt% H_3PO_4 to a 3 M V(V) / 5 M H_2SO_4 solution increased the induction time of V(V) precipitation from 3 days (blank) to 47 days; higher concentrations (2-3%) were found to have little beneficial impact. Kausar et al. [60] observed that with the addition of 1% phosphoric acid to the VRFB electrolyte, induction times of 40, 22, and 18 days were achieved for 80, 90, and 95% SOC solutions at 50 °C, compared with 5, 2 and 1 days, respectively, for the corresponding blank solution. More recently, Yeon et al. [61] investigated the effect of sodium pyrophosphate dibasic (SPD) on the stability of 2 M V(V) / 3 M H_2SO_4 at 40 °C and found that precipitation could be delayed from 12 days (blank) to 336 days with 0.1 M SPD; charge–discharge experiments carried out for over 500 cycles also showed significant improvement in capacity retention. Further studies by Rahman and Skyllas-Kazacos [62] found that a blended additive formulation consisting of 1 wt% K_3PO_4 and 1 wt% $(NaPO_3)_6$ could delay the induction time of V(V) precipitation from 3 days (blank) to 40 days in a supersaturated 4 M V(V) / 6 M total sulfur solution at 40 °C. The group also observed that, although increasing the total sulfate increased V(V) stability, it also exponentially increased viscosity, likely due to the formation of electrochemically inactive vanadium-sulfate and polyvanadic complexes; the increase in viscosity translated to a marked decrease in electrochemical activity.

Although considerable progress has been made in terms of precipitation inhibitors for supersaturated electrolyte, the majority of research is still preliminary, in that it focuses on *ex-situ* experiments with either the anolyte or catholyte. Only a few research groups have substantiated their findings with *in-situ* cycling tests involving additives in both half-cells and, even so, experiments are rarely performed past 100 cycles. As such, there is an open opportunity for further work to identify precipitation inhibitors that improve capacity retention over the long term in an operating VRFB.

2.1.4.2 Alternative electrolytes

To ensure long electrolyte life, alternative aqueous and nonaqueous solvents and supporting electrolytes may create a new pathway to high energy density and more thermally stable chemistries. As with the precipitation inhibitors above, to ensure long electrolyte life, any new chemistry requires the same active material in both half-cells in order to prevent diffusion across the membrane.

Lee et al. [63] developed a novel cathodic V(IV)/V(V) electrolyte based on oxalic acid ($H_2C_2O_4$). This $H_2C_2O_4$-based electrolyte considerably improved both reaction kinetics as well as redox reversibility, resulting in remarkable charge–discharge capacities. It was theorized that the high charge–discharge capacities resulted from the redox reaction of both $V(Ox)^{2-}$/ $V(Ox)^{-}$ (vanadium chelate) and $[VO(H_2O)_5]^{2+}$/$[VO_2(H_2O)_4]^{+}$ couples in the catholyte. Although the use of $H_2C_2O_4$-based electrolyte offers a potentially useful approach to prevent electrolyte degradation and enhance cell performance, further studies are still required in terms of long-term stability, the reaction mechanism, and the possibility of organic decomposition.

Vijayakumar et al. [64] investigated the V(V) cation structures in mixed acid (hydrochloric and sulfuric) based electrolyte via computational modeling. The results showed that, at higher

vanadium concentrations (≥1.75 M), V(V) exists as a di-nuclear $[V_2O_3Cl_2{\cdot}6H_2O]^{2+}$ compound which can be resistant to de-protonation and the subsequent V_2O_5 precipitation. It was also found that an increase in temperature facilitated the formation of this di-nuclear compound and, therefore, the thermal stability of V(V) cations in mixed acid system could be enhanced.

More recently, Oldenburg et al. [65] expanded on the knowledge that H_3PO_4 was beneficial as a V(V) precipitation inhibitor and tested a 2 M H_2SO_4 / 1 M H_3PO_4 mixed electrolyte. Preliminary cycling results revealed a 7% increase in voltage efficiency (VE) when compared to the equivalent purely sulfuric acid- supported electrolyte. However, cycling was brief and the vanadium concentration was only 1 M and, therefore, further testing is required to determine the true potential of this alternative.

Other supporting electrolytes, such as methanesufonic acid, have also shown promising results; however, most are more expensive than H_2SO_4 and are therefore cost-inhibitive.

2.1.4.3 Electrolyte additives

For improved performance and stability, substantial research has been conducted in terms of electrolyte additives.

The influence of various additives on the stability of V(V) electrolyte was studied by Wang et al. [66]. The group investigated the stability of V(V) electrolyte with and without additives over a temperature range of -5 °C to 60 °C and found that methyl orange, Triton X-100, sodium ligninsulfonate, sodium dodecyl sulfate, and polyvinyl alcohol all generated significant improvements. In addition, all of these additives also displayed improved electrochemical activity when compared to the pristine solution.

Ding et al. [67] investigated a series of phosphates as additives to improve the stability of VRFB electrolyte. It was demonstrated that $NH_4H_2PO_4$ significantly improved both the reversibility and activity of the redox reaction, while also increasing the energy efficiency. Further, the cell with $NH_4H_2PO_4$ additives in the electrolyte exhibited a much slower charge capacity fading rate in comparison to the cell without additives during cycling at high temperature. The results indicate that the long-term stability and durability of VRFBs are improved by the phosphate additives, reducing the electrolyte maintenance cost for long-term operation.

2.1.4.4 Electrochemical means

Sometimes, the precipitation of vanadium ions is inevitable due to unexpected temperature drift, supersaturation, or the formation of intermediate species. Once precipitation occurs, the V(II), V(III), and V(IV) salts may be redissolved by increasing the temperature. However, this strategy does not apply to any V(V) precipitate that might form at elevated temperatures. In this case, electrochemical means may be employed to redissolve any V(V) precipitate. Such means may include reversing the cell polarity to convert V_2O_5 into V(IV) or V(III) or partially mixing the charged anolyte and catholyte to allow V(II) to electrochemically leach solid V(V) back into solution [24].

2.2 Membrane

2.2.1 Functions and properties of membranes

The VRFB membrane is a semipermeable membrane generally made from ionomers or polymers. It is designed to be a separator between the anode and cathode compartments to separate the active

species. In the meantime, it also acts as an electronic insulator and an ionic conductor, facilitating the transport of ions such as protons or sulfate ions to maintain charge balance within the cell. The demands for the membrane are stringent: high ion exchange capacity or high ionic conductivity, low vanadium ion permeability, low cost, optimal water transfer properties, and long-term chemical stability under VRFB operating conditions. A high proton conductivity and low vanadium ion crossover could improve VRFB's coulombic efficiency (CE), leading to high overall efficiency. Optimal water transfer properties could avoid precipitation of vanadium salts in the cell and flooding of the solution reservoir. Long term chemical stability of the membranes in charged electrolyte solutions is of great importance for the durability of VRFBs.

In general, membranes can be classified based on factors such as the nature of the material, morphology, and pore size. According to the type of ionic functional groups attached to the membrane backbone, ion exchange membranes can be categorized into cation exchange membranes (CEMs), anion exchange membranes (AEMs) and amphoteric ion exchange membranes [68]. Cation exchange membranes contain negatively charged groups, such as $–SO_3^-$, $–COO^-$, $–PO_3^{2-}$, $–PO_3H^-$ and $–C_6H_4O^-$. They provide passages for cations, such as Na^+, whereas they are non-permeable to anions like Cl^-. Anion exchange membranes have positive functional groups, such as $–NH_3^+$, $–NRH_2^+$, $–NR_2H^+$, $–NR_3^+$, and $–SR_2^+$, and thus allow the passage of anions. Amphoteric ion exchange membranes, also called bipolar membranes or composite membranes, can be produced to contain a cation selective layer (with negative fixed ionic groups) and an anionic selective layer (with positive ionic groups).

Various membranes have been investigated for VRFB applications. Currently, the most widely used are Nafion® membranes; however, they have several disadvantages, such as high cost (US \$200-500/m^2) and high vanadium crossover. In order to reduce the cost and extend the lifetime of VRFB membranes, great efforts have been made by researchers in the VRFB research and development community. In addition to modifying Nafion® membranes [69][72], alternative membranes have also been developed, including other polymeric CEMs, such as polyether ether ketone (PEEK) [68] and sulfonated diels-alder poly(phenylene) [73], AEMs [74][75], amphoteric ion exchange membranes [76][78], and microporous separators such as Daramic membranes and Amer-Sil membranes [79][82]. Even if modifying Nafion® membranes could enhance the chemical stability, it would not reduce the overall cost of the membrane itself; thus, research efforts are being focused on alternative perfluorinated acid membranes, new anion-exchange membranes, and other types of polymer membranes.

2.2.2 Membrane degradation mechanisms

The VRFB is known to degrade in performance over time. Membrane degradation in extreme chemical environments is one of the major factors leading to reduced capacity or increased internal resistance. The crossover rate of vanadium ions through the membrane, water transport property, and chemical stability of the membrane strongly affect the membrane durability in VRFBs.

2.2.2.1 Vanadium ions crossover

Vanadium ion crossover represents the diffusion of vanadium ions across the membrane, which will lead to self-discharge and side reactions at the positive and negative electrodes, affecting the VRFB capacity over long term charge–discharge cycling. Depending on the SOC, the catholyte contains a mixture of V(IV) and V(V) ions while the anolyte contains V(III) and V(II) ions. This results in concentration gradients of each ion across the membrane, motivating the diffusion of

each species from one half-cell to the other during cycling. The rate of crossover of the vanadium ions provides an insight on how to optimize operating conditions to reduce the crossover of vanadium ions and thus enhance the durability of VRFBs.

Agar et al. [83] used a 2-D transient model to study the ion transport mechanisms responsible for vanadium crossover of VRFBs. It was found that the immediate crossover of vanadium across the membrane during cycling caused side reactions which negatively affected the battery's CE. The magnitude of the vanadium ion diffusion determines the rate of the self-discharge reactions. Even if the vanadium transport during charging is exactly equal to the vanadium transport during discharging in the opposite direction, the cell will not maintain 100% CE. The side reactions associated with species crossover is listed in Table 2 [84].

Table 2

Zhang's group [84][85] found that the vanadium crossover was closely related to the self-discharge of VRFBs. They also found that the crossover of vanadium ions was mainly due to the concentration difference of vanadium ions between the catholyte and anolyte, leading to a decreased OCV value as long as the electrolyte flows continually at both sides of the membrane.

Vanadium ion crossover is also accompanied by other ions to maintain electric neutrality, leading to capacity decay. Sun et al. [86] investigated the transfer behavior of different ions across the VX-20 AEM and the Nafion® 115 CEM in an operating VRFB. It was found that V(II) ions accumulated at the negative side when using Nafion® 115, while the V(IV) ions accumulated at the positive side with VX-20. To balance the charges, the SO_4^{2-} ions transferred across the Nafion® 115 while the protons transferred across the VX-20 membrane. The mechanisms of capacity decay were also found to be different between the two membranes; for Nafion® 115, cross mixing of vanadium ions through the membrane was the major contributor, while for VX-20 the side reactions were the main cause. Figure 2 shows the diagrams of the ion transfer between the positive and negative sides of the membrane [86]. Note that the diagrams give an overall direction only. During operation, the transfer direction could be different during the charge and discharge processes.

Figure 2

Convection, resulting from electrolyte hydraulic pressure differentials at both sides of the membrane, is also considered to have a dominant effect on vanadium crossover and capacity decay while cycling. Li et al. [87] studied the capacity decay mechanism of VRFBs using microporous separators as membranes. They determined that the capacity decay was due to the disproportionate valance of vanadium ions caused by unbalanced self-discharge reactions on either side of the membrane. Although the total vanadium concentration remained relatively constant on both sides over cycling, a net transfer of electrolyte from one side to the other was observed. Nevertheless,

the rate of vanadium permeation through the membrane was very small in comparison to the transport rates associated with migration under current.

Some mathematical modeling work has been done to simulate the accumulation of vanadium ions and predict the capacity loss over the course of many cycles. For example, Skyllas-Kazacos et al. [88] modeled the concentration profiles of vanadium ions across a CEM as a function of time under various charge and discharge currents. The model predicted an accumulation of vanadium ions in the positive half-cell, in agreement with prototype observations in the laboratory. This proved that asymmetrical rates of diffusion across the membrane lead to capacity loss resulting from an increase of vanadium ions in one half-cell with a corresponding decrease in the other. Through a 45-cycle simulation of both Nafion® and s-Radel CEMs, Agar et al. [83] also observed a net transfer of vanadium from the negative to positive half-cell, which was responsible for the loss in capacity. They concluded that the operating conditions, together with diffusion, convection, and migration could significantly influence the rate and direction of crossover during the VRFB operation. For the case of the two CEMs, their model output indicated that convection was the largest contributor to species transport. The modeling work of Elgammal et al. [89] propounded that, under current, the transport rates associated with migration was much higher than the rate of vanadium permeation through the membrane.

In general, the state of vanadium electrolyte and the transfer behavior of different ions are closely related to the ion exchange membranes. The characteristics of membranes, e.g. the functional charged groups, the backbone, the micro structures, greatly affect their transfer behaviors.

2.2.2.2 Water transfer

Water transfer is another important source of performance degradation over cycling either due to precipitation of vanadium salts or flooding of the electrolyte reservoir [90]. There is a net volumetric water transfer across the membranes during charge–discharge cycling of the VRFB and studies have shown that the direction of the volumetric transfer is dependent upon the nature of the ion exchange membrane used [90][91]. For a cell employing an AEM, it was observed that the net volumetric water transfer is toward the negative half-cell, whereas for CEMs the net volumetric water transfer is toward the positive half-cell.

The direction of water transfer is also dependent on the SOC of the vanadium electrolytes employed. Sukkar et al. [90] reported that when the electrolyte self-discharged from 100 to 50% SOC, the water migrated in the direction of the positive half-cell. As the electrolyte discharged further from 50 to 0% SOC, the water transfer reversed direction toward the negative half-cell. When the cell over-discharged below 0% SOC, i.e. where the V(III) and V(IV) electrolytes become fully mixed, the observed water transfer toward the negative half-cell was the most significant.

Water transfer across the membrane can be caused by a number of processes including water transported alongside vanadium ions, electro-osmotic drag, and diffusion via osmotic pressure difference between the two half-cell solutions. The contribution from each process varies for different membranes and vanadium electrolytes, giving a different level of net water transfer for each membrane [91]. Recently, Oh et al. [92] developed a model to study both the direction and mechanisms of water transport within a VRFB. The model, which compared well against *in-situ* charge–discharge experiments, indicated that diffusion, electro-osmotic drag, and consumption/production from the V(IV)/V(V) redox couple were the main contributors to water transport. Although electro-osmotic drag caused large changes in volume, the net transfer during

a single cycle was near zero; water transfer due to diffusion, however, was found to be unidirectional during cycling and therefore the primary cause of electrolyte imbalance. These results may provide insight for future research efforts, where reduction in diffusion could be the main focus.

2.2.2.3 Membrane chemical stability

The membrane's chemical stability plays an important role in the service life of a VRFB due to the harsh chemical environment. Many materials cannot withstand the high concentration of supporting H_2SO_4 and the strong oxidation potential of V(V). It is important, therefore, to both study and understand the mechanisms of membrane degradation in this environment.

Mohammadi et al. [93] studied the chemical stability of Daramic, modified Daramic, and commercial ion exchange membranes during charge–discharge cycling by monitoring the membrane resistivity and permeability to identify any changes due to membrane fouling or degradation. It was found that chemical degradation is linked with the oxidation of the polymeric membrane material by the catholyte.

When Sukkar and Skyllas-Kazacos [94] studied the membrane stability, they found that the resistivity of membranes decreased after extended exposure to a 0.1 M V(V) + 0.25 M H_2SO_4 solution, possibly due to erosion of polymeric material. The ion exchange capacity (IEC) of membranes was found to increase with soaking time; this might be attributed to SO_4^{2-} and HSO_4^- from the solution being embedded in the pores of the membrane. The V(IV) ion diffusivity of membranes was also found to be adversely affected by extended exposure to the solution. The results from the long-term stability tests indicated that the faster rate of ion transfer should likely take the credit for the decrease in resistance of the membrane and, although the weight loss and degree of oxidation was low, all of the membrane properties gradually deteriorated over time.

Huang et al. [95] studied sulfonated polyimide (SPI) membrane degradation in VRFBs. They found that, after 800 cycles, the SPI membrane was visibly fractured, resulting in the VRFB failure. Optical and SEM examinations of the membrane showed that the membrane surface facing the positive electrode contained considerable microdefects, while the surface facing the negative electrode did not change, as shown in Figure 3. The highly oxidative V(V) species and strong acidic environment were considered to be responsible for the membrane degradation; evidence of this comes from the generation of V(IV) (the reduction product of V(V)) observed alongside degradation. In their studies, the higher the concentrations, the faster the membrane degradation. Kim et al. [96] investigated the chemical degradation of a sulfonated poly(sulfone) membrane during charge–discharge cycling in the VRFB cell. They found that the membrane experienced delamination on the surface facing the positive electrode, akin to the observations by Huang's group. Both vanadium-rich and sulfur-deficient regions were observed near the degraded surface.

Figure 3

Noting the lack of understanding of the degradation mechanisms of hydrocarbon membranes, Choi et al. [97] recently studied a series of sulfonated poly(ether sulfone) copolymers. They observed that polymers designed with electron-withdrawing sulfone linkages had significantly better

stability than those with electron-donating thioether linkages. It was theorized that the linkage groups in the latter membrane were more flexible, thus allowing the V(IV) ions to pass through the membrane more easily. Publications describing the degradation mechanism of AEMs are also scarce. Those that do exist have reported the attack of positively charged functional groups by V(V), rendering the membrane neutral and shifting the electrophilic center to the polymeric backbone where further attack takes place, ultimately leading to the scission of the main chain [98].

Chemical stability tests have become a standard for most research groups studying membranes for VRFB applications; however, most report binary results: either the membrane degraded or it didn't. Only a percentage conduct detailed investigations in an attempt to identify the precise mechanisms of membrane degradation. As such, there is still much to be learned and discovered in this area.

2.2.3 Diagnostic tools for membrane degradation

2.2.3.1 Vanadium ions crossover measurement

The crossover of vanadium ions cannot be avoided if electrolyte flows continuously at both sides of the membrane. The vanadium ions that do cross over could cause undesired contamination and energy losses in the VRFB system. To predict the VRFB degradation, it is crucial to measure and quantify these crossover rates.

Heintz et al. [99] built a dialysis cell consisting of two half-cells separated by the membrane to measure the diffusion coefficients of vanadium ions; atomic absorption spectrometry and ion chromatography were used as analytical tools. For this work, experimental data obtained from exchange diffusion and ion exchange equilibria measurements were used to determine the diffusion coefficients, and thus ultimately the diffusion velocity, of the ions in the membrane.

A standard test procedure to measure vanadium ion crossover was developed by Skyllas-Kazacos and co-workers [68][94]. To eliminate any interference from water transport due to osmotic pressure effects across the membrane, *ex-situ* testing procedures were also developed [68][84][85][94]. Typically, the membrane is sandwiched between two half-cells with gaskets on either side to prevent solution leakage [89]. One half-cell contains $VOSO_4$ solution, and the other half cell contains $MgSO_4$ solution. The $MgSO_4$ solution is sampled periodically to measure the increasing V(IV) concentration using a UV/Vis spectrophotometer; from this, the permeability of the V(IV) ions through the membrane can be calculated. The diffusion rate of V(IV) is determined by the absorbance rate change according to the following equation [68].

$$\ln[absB_0 - 2absA] = \ln[absB_0] - \frac{2k_s At}{V_A} \tag{11}$$

where $absB_0$ is the initial absorbance of solution B, absA is the absorbance of solution A, A is the area of the membrane exposed, t is time, and V_A is the volume of solution A. The slope of a plot of $\ln[absB_0 - 2absA]$ versus t determines the mass transfer coefficient (k_s) of the V(IV) ions across the membranes. The plot should be linear and has a slope equal to $-2k_sA/V_A$. The diffusion coefficient, D, can then be calculated using the following equation:

$$D = k_s dy \tag{12}$$

where y is the thickness of the membrane. Diffusion coefficients of vanadium ions have been reported in the range of $\times 10^{-5}$ to $\times 10^{-4}$ cm min^{-1} for Nafion® 117 while other membranes have ranged from $\times 10^{-6}$ to $\times 10^{-2}$ cm min^{-1} [100].

The method developed by Skyllas-Kazacos' team is widely used by researchers and can be found in most research papers studying VRFB membrane permeability. Such a wide adoption of the procedure allows for direct comparisons (providing similar solution concentrations are used) of independent *ex-situ* studies and gives more weight to the findings. This measurement is, therefore, an excellent first step in membrane evaluation; however, it is not fully representative of the actual operating conditions that the membrane will experience. For example, the procedure involves only one of the four valence states of vanadium that the membrane will be exposed to during cycling and, therefore, does not depict the crossover rates of the other ions. To supplement this test, an additional method of vanadium transport can also be measured during VRFB operation. For this measurement, periodic samples of both anolyte and catholyte can be taken either at the end of a cycle or at both the charged and discharged states; the samples can be subsequently titrated to determine the change in vanadium ions concentrations.

2.2.3.2 Water transfer measurement

A standard *ex-situ* water transfer test cell was developed [68] to monitor the net water transfer across the membrane. The cell contains two half-cells, each with a cavity for solution, and clear tubes to monitor liquid level. The test membrane is fixed between the two half-cells. The test begins with the solutions at the same level, from which the deviations are recorded periodically over time.

As with the *ex-situ* vanadium crossover measurement in the prior section, this water transport test is effective for preliminary screening of membranes, but may not simulate the actual rates in an operating VRFB. Identifying this gap, Sun et al. [84] developed a method to test water transfer across Nafion® 115 membrane in an operating VRFB stack. They studied water transfer during both cycling and self-discharge. In the cycling experiments, the stack was charged to an upper limit voltage of 1.55 V per cell and discharged to a lower limit of 1 V per cell for each cycle. The volume of catholyte and anolyte were recorded every 10 cycles. For the self-discharge test, after charging to 1.55 V per cell, the stack was left with pumps running to initiate a dynamic self-discharge process. The volume of catholyte and anolyte were recorded every few hours to measure the water transfer across the membrane.

2.2.3.3 Chemical stability test

For membrane stability evaluations, *ex-situ* immersion of membranes in V(V)-containing electrolyte is the most direct and effective method, especially at elevated temperatures which accelerate the chemical degradation of the membrane and shorten the experimental duration. Typically, a pre-weighed membrane with a known area is soaked in a known volume of V(V) solution. Membrane oxidation by V(V) ions produces blue V(IV) ion species, which is used as an indicator for the membrane stability measurement. V(IV) concentration can be determined by UV/Vis spectrophotometry or by titration. By periodically monitoring V(IV) absorbance, the membrane oxidation rate can be obtained [94]. The membrane weight loss can also provide insight towards the chemical stability.

The immersion test has both advantages and disadvantages. It is a simple and straightforward method to implement and results are visibly evident, which is likely why so many researchers have utilized this procedure for their evaluations. However, the same researchers have used a wide range of solution concentrations for their measurements, rendering a challenge for direct comparisons to other studies. In addition, while this method determines chemical stability, it does not provide any

insight towards the mechanisms taking place to cause the degradation. Therefore, it is suggested that other spectroscopic measurements such as Fourier-transform infrared spectroscopy (FTIR), SEM/EDS, or NMR are used to supplement the test.

2.2.4 Mitigation strategies of membrane degradation

In terms of membrane degradation, several strategies have been applied to mitigate vanadium crossover, water transport, and loss of chemical stability.

2.2.4.1 Modification of Nafion®

The instantaneous transport of vanadium across the membrane during charge and discharge can be mitigated by minimizing imbalances of species concentration between half-cells during cycling, thereby extending the lifetime of a VRFB. This requires further control of the specific transport properties of the membrane. As such, hybrid and composite membranes have been functionalized to extenuate vanadium crossover.

Cha et al. [69] reviewed recent developments of nanostructured membranes for VRFBs. Modifications of Nafion® seem to be effective in decreasing vanadium crossover; for example, coating Nafion® with a cationic charged layer was found to reduce the permeation of vanadium ions [70]. Comparing the modified membranes with pristine Nafion®, it was observed that the modification dramatically reduced the crossover of vanadium ions through the membrane with only a slight increase in resistance in return. Another approach involved the fabrication of a barrier layer onto the surface of Nafion® by using an alternate absorption polyelectrolyte layer-by-layer self-assembly technique [71]. This barrier layer significantly suppressed the crossover of vanadium ions, as shown by the self-discharge results. Skyllas-Kazacos et al. [68] reported that a Nafion®/inorganic oxide nanoparticle hybrid membrane could significantly reduce vanadium ion permeability. Compared to pristine Nafion®, the hybrid membrane exhibited a lower self-discharge rate with improved coulombic, energy, and voltage efficiencies. Polymer blending is also an effective method for polymer modification. Inspired by the performance of Nafion®/polyvinylidene fluoride (PVDF) for fuel cell applications, Mai et al. [72] investigated the feasibility of this blended membrane for VRFB systems. The highly crystalline and hydrophobic PVDF seemed to effectively control the swelling of Nafion®, resulting in higher efficiencies, lower crossover, and improved self-discharge rates.

As described above, significant improvements can been made to Nafion® membranes in order to counter vanadium crossover and the resultant effect on overall VRFB performance. These improvements, however, do nothing to counter the high cost of the membrane itself. With high cost being one of the main obstacles limiting VRFB commercialization, it is necessary to find a low-cost alternative.

2.2.4.2 Alternative membranes

To achieve a lower vanadium crossover and better chemical stability, the fluorinated CEM has received some attention in the research community. Wei et al. [101] have demonstrated that PVDF ultrafiltration membranes presented comparable performance to Nafion® with the benefit of exceptional stability observed over 1000 cycles. A low-cost poly(vinylidene fluoride)-graft-poly(styrene sulfonic acid) (PVDF-g-PSSA) CEM was prepared by Luo et al. [102] using a solution-grafting method. Due to the high conductivity and extremely low vanadium ion permeability measured, the VRFB test results exhibited a higher performance compared to Nafion®

117 under the same operating conditions. The VRFB performance with the PVDF-g-PSSA membrane was found to be stable over the nearly 250 cycles tested. Another partially fluorinated CEM was prepared by Qiu et al. [103] via radiation grafting of styrene and maleic anhydride onto the PVDF membrane followed by sulfonation. The grafted membrane exhibited a much lower permeability than Nafion® 117. Moreover, the OCV during dynamic self-discharge was maintained above 1.3 V for more than twice as long as Nafion®.

More recently, hydrocarbon-based AEMs have been considered for VRFB applications since they offer solutions to many of the problems found with Nafion® such as high vanadium crossover and capacity decay. For example, Sandia National Laboratories reported the development of poly(phenylene) membranes showing promising results with respect to performance and durability [104]. Zhou at al. [105] found that polybenzimidazole (PBI) membranes were advantageous over Nafion® 211 at maintaining capacity. The PBI-based VRFB maintained a capacity decay rate four times lower than that of the Nafion®-based VRFB due to the extremely low vanadium ion permeability. A cross-linked pyridinium functionalized poly(2,6-dimethyl-1,4-phenylene oxide) (PPO) membrane was fabricated by Zeng et al. [106] to address the issue of low chemical stability for VRFBs. The modified PPO membrane demonstrated exceptional chemical stability in both the *ex-situ* immersion test as well as the continuous cycling test. Under high current conditions, the PPO-based cell maintained 80% of the initial discharge capacity across more than 500 cycles.

Table 3 summarizes the results of the alternative membranes compared to Nafion®.

Table 3

In addition to membrane modifications or alternative membranes, membrane thickness adjustment could be another way to obtain extended lifetime for VRFBs. Research has shown that performance can be significantly improved by optimizing membrane thickness for specific operational conditions [107]. However, these results were only applicable to the one CEM tested and further study is necessary to corroborate the findings.

Although the alternative membranes described above show encouraging results towards improving capacity retention, most revealed significantly lower conductivity in comparison with Nafion® and thus require further refinement before they can be used in practical applications. Improvement of chemical stability is also warranted; although some alternative membranes were reported to be durable, many of the tests utilized electrolyte concentrations lower than those typically used in operating VRFBs.

2.3 Electrode

The electrode is one of the key components of VRFBs, providing active sites for the reaction of redox couples. The essential requirements of a suitable electrode for VRFB applications include electrochemical stability in the operation potential window, chemical stability in highly acidic environments, high oxygen and hydrogen overvoltage, and excellent electrical conductivity for fast charge transfer reactions. The electrode degradation has been found to account for a major portion of the overall performance loss. For example, Derr et al. [108][109] estimated that, across 50 cycles, the overall performance loss was between 60-75%, 10-55% of which was constituted

by electrode degradation, while the remaining losses were accredited to ohmic loss and the imbalance of the electrolyte.

2.3.1 Electrode materials

The history of electrode development for VRFBs has been summarized by Kim et al. [27] with a vivid historical flow chart provided. A variety of carbon materials, including CF, GF, carbon nanofibers, carbon nanotubes, carbon paper, and graphene oxide have been widely investigated as electrodes for VRFBs. Composite electrodes have also been investigated as bipolar electrodes by blending carbon materials with polymers. Owing to the high electrical conductivity, excellent chemical stability, three-dimensional network structure, a large specific surface area, and wide operation potential windows, carbon and graphite felt materials are most commonly used and well-suited for both the positive and negative half-cells in VRFBs [27].

The electrochemical reactions take place on the carbon electrodes. In the meantime, the mass transfer of ions/protons and the transport of electrons to/from the active sites of the electrode also occur. The performance of the electrode strongly depends on the properties of the carbon materials used, including chemical stability, electrochemical activity, electrical conductivity, and porosity [6].

In general, carbon and graphite electrodes were found to function well under normal charge–discharge cycling conditions with a slow degradation. In varied abused conditions, degradation of the electrode may severely occur.

2.3.2 Electrode degradation mechanisms

Degradation of carbon materials in VRFBs is a complex issue. During the lifetime of an operating VRFB, carbon-based electrodes may suffer degradation from sources such as electrochemical, mechanical, and thermal [110]. Likely, a combination of different effects may also be responsible, including material properties and surface chemistry, hydrogen evolution, and mass transport. To gain an overview of factors contributing to electrode stability and degradation in VRFBs, this section summarizes the main degradation mechanisms of the electrode although, so far, there is limited work which takes into account the degradation of the electrodes. Note that the dominant mechanism behind degradation for each case will depend on the operating conditions of the VRFB.

2.3.2.1 Mechanical and thermal degradations

Mechanical degradation often refers to the mechanical stripping of the electrode, which, in turn, brings decreased active surface areas, blocked pores, or increased stresses in the carbon electrode [110]. Kim et al. [27] commented on early-days testing using carbon cloth for VRFB electrode material; in this case, a high rate of mechanical degradation occurred during charging. In hindsight, they attributed this to the low surface area of the carbon cloth and the flow-by configuration in comparison with the flow-through operation when using CFs as electrodes, thereby limiting the diffusion of vanadium ions and increasing oxygen evolution during charging. Due to the inevitable mechanical degradation, carbon cloths have not been widely studied for use as VRFB electrode materials.

To ensure the long-term durability of VRFBs, the mechanical properties of the bipolar carbon materials must be considered in addition to their chemical stability, electrochemical properties, and electrical conductivity. This explains why significantly thick CFs, with a thickness in the mm

range, is usually employed in VRFB applications, unlike the gas diffusion layer, with a thickness in the µm range, in PEM fuel cells. The thick CF absorbs the stress of the assembly and serves as a connector for the electrical contacts. A thicker CF also enhances diffusion lengths, which can reduce the overall resistance [110].

Thermal degradation of the electrode is commonly caused by thermal differences within the electrode. Depending on the load, current densities may be localized, inducing thermal differences within the carbon microstructure coupled with mechanical/thermal processes during the cell charge–discharge operation. Consequently, mechanical and thermal expansions of carbon may occur due to thermal differences within the electrode. Chemical reaction rates may also be affected. The thermal differences within the electrode could also provoke regional failure in the electrode. Unfortunately, limited work has been done in this field as identifying the causes and understanding the mechanisms is not an easy task [110].

2.3.2.2 Electroless chemical aging

Electroless chemical aging of the electrodes occurs due to chemical reactions of the felts with sulfuric acid or/and with vanadium. Without applying a current or voltage, sulfuric acid, as well as vanadium in the electrolyte, can chemically react with the CFs. This electroless aging, also referred to as chemical aging, was found to be inevitable for all types of CFs commonly used.

So far, literature on the aging of VRFBs is scarce, with research on the chemical aging of electrodes being even more so. Derr et al. [111] studied electroless aging of CF electrodes by soaking them in electrolyte for a certain time period and temperature. Without applying any potential, the electrolyte-induced chemical degradation of the felts could then be investigated in both half-cells. Electrochemical impedance spectroscopy (EIS) analysis demonstrated that the aging of the carbon electrodes was associated with the temperature as well as vanadium concentrations. Experiments showed that chemical reactions of the CF with both sulfuric acid and vanadium occur. The three-electrode experiments also confirmed chemical aging under real VRFB operating conditions. X-ray photoelectron spectroscopy (XPS) indicated similar changes to the surface of CFs at both the positive and the negative electrodes. The amount of oxygen functional groups increased while the amount of sp2-hybridized carbon decreased after 8 days of chemical aging. Results also showed that the negative electrode was more strongly affected by chemical aging than the positive electrode for a duration of up to 30 days.

2.3.2.3 Electrochemical degradation

The most recognized degradation mode for the carbon electrode is electrochemical degradation, also known as carbon corrosion under acidic environment. For the durability of VRFBs, electrochemical degradation of CF electrodes appears to be a key issue. In the positive half-cell, possible electrochemical reactions include the oxidation of carbon to CO_2 and the oxygen evolution reaction (OER). In the negative half-cell, the hydrogen evolution reaction (HER) competes with the V(II)/V(III) reaction. Almost exclusively, the electrochemical side reactions take place during the charging process, resulting in a decrease in electrochemical surface area (ECSA), as well as activity towards vanadium redox reactions [108].

In the positive half-cell of VRFBs, the carbon electrode is easily corroded because of CO_2 evolution. Under normal conditions, such as during VRFB discharge, the potential is less than 1.4 V and the carbon electrode remains stable. However, during charging, the positive electrode

potential is as high as 1.8 V; under this high potential, the following reactions may occur at the positive electrode:

$$C + H_2O \rightarrow CO + 2H^+ + 2e^- \quad (13)$$

$$CO + H_2O \rightarrow CO_2 + 2H^+ + 2e^- \quad (14)$$

$$2H_2O \rightarrow O_2 + 4H^+ + 4e^- \quad (15)$$

Due to the change in the surface functional groups or the loss of ECSA at the electrode, these heterogeneous side reactions could cause performance degradation of the electrode. As well, these side reactions consume current densities, and thus may lower the energy efficiency of a VRFB. Also, bubbles formed during the side reactions weaken the effective contact between electrolyte and electrode, reducing the active surface area for redox reactions and disturbing the transport of the reactants. By controlling the applied potential difference, gas evolution may possibly be supressed. In addition, due to asymmetric internal resistance, local potential and temperature may rise in the cells. As a result, gas evolution in localized regions may occur and the felt electrode corrosion may be expedited due to the decrease in the OER overpotential caused by the increase in temperature [112].

In the negative half-cell of VRFBs, the HER (Equation (16)) has a very strong impact on the performance of the negative electrode. The evolution of hydrogen not only consumes current but also damages the carbon fibers.

$$2H^+ + 2e^- \rightarrow H_2 \quad (16)$$

Side reactions of O_2 and CO_2 evolution were observed by Liu et al. [112] and the corrosion behavior was investigated. When the graphite electrode acts as the positive electrode, it easily suffers from electrochemical degradation because of CO_2 and O_2 evolution. Using potentiodynamic and potentiostatic techniques, the effects of polarization potential, operating temperature, and polarization time on graphite corrosion were investigated. The results showed that when the anodic potential was higher than 1.60 V vs. saturated calomel electrode at 20 °C, CO_2 and O_2 evolution occurred on the graphite electrode; and when the polarization potential reached 1.75 V, CO_2 evolution on the graphite electrode could cause intergranular corrosion of the graphite. In addition, they found that functional groups of COOH and C=O on the electrode surface could catalyze the evolution of CO_2, thereby accelerating the corrosion of the electrode.

Derr et al. [108][109] studied electrochemical degradation of electrodes during both cycling experiments and half-cell measurements at various SOCs. As part of their research, XPS revealed that the oxidation of carbon occurred at both half-cells in a similar manner. SEM depicted a peeling of the fiber surface after cycling, resulting in a loss of ECSA. Based on the cycling experiments, it was found that the degradation rate strongly depended on the cycling conditions, including the cut-off voltage and the experiment duration. The higher the cut-off voltage, the faster the electrode degraded. During the cycling experiments, they found that electrochemical degradation was influenced by chemical aging and that electrochemical degradation had a stronger impact on the negative half-cell than the positive half-cell. This implies that the negative half-cell is rate determining for the VRFB and, therefore, modification of the positive carbon electrode does not significantly affect the VRFB performance.

Based on results from electrochemical degradation investigations, and even preliminary chemical aging tests, it is evident that the CF at the negative half-cell is notably more sensitive to changes at the electrode surface and is, therefore, much more prone to degradation. As such, it is recommended that future tests of CF material modifications or degradation mechanisms focus more heavily on the impact to the negative electrode.

2.3.3 Diagnostic tools for electrode degradation

Given the significant influence of electrodes on the performance of VRFBs, it is very important to understand the factors affecting their performance degradation and under which conditions the electrode becomes severely eroded. Thus, techniques should be identified to determine the micro- and nano-scale degradation mechanisms of carbon-based electrodes so that proper mitigation strategies can be applied.

2.3.3.1 Electrochemical tools

Electrode performance and degradation within a VRFB can be evaluated by electrochemical techniques such as EIS, linear sweep voltammetry, cyclic voltammetry (CV), and cell charge–discharge cycling.

EIS is a useful tool to monitor changes in ohmic resistance, double layer capacitance, and charge transfer resistance. The main advantage of EIS over cyclic voltammetry is the low current/voltage required during the measurement; at such low loads, parasitic reactions like the HER can be neglected. Using the EIS results shown in Figure 4, Sun et al. [113] developed a technique to obtain the ohmic, charge transfer, and diffusion overvoltages at the negative electrode of a VRFB. The voltage losses at different flow rates and electrode thicknesses were quantified as a function of current density during both charge and discharge. Results showed that the diffusion overvoltage was strongly influenced by flow rate while the charge transfer and ohmic losses were unaffected. A Tafel plot was obtained using the impedance-resolved charge transfer overvoltage; from this, parameters such as the geometric exchange current density, anodic and cathodic Tafel slopes, and corresponding transfer coefficients were then determined.

Figure 4

Liu et al. [114] studied graphite corrosion and found via linear sweep voltammetry that, in a pure H_2SO_4 solution, graphite started to oxidize at 1.15 V, while in the presence of $VOSO_4$, the onset potential of carbon oxidation shifted to 0.9 V as shown in Figure 5.

Figure 5

CV can be used to identify vanadium redox peaks, compare anodic and cathodic current densities of electrodes, determine the reversibility of the redox couple, evaluate long-term stability, and quantify the ECSA, an important indicator of the electrode performance. Wu et al. [115] studied the performance of GF electrode treated by two different methods: thermal treatment and modified

Hummers method. Figure 6 shows the CVs of the GF electrodes. The thermally treated GF exhibited lower oxidation and reduction peak current densities compared with those for the GF treated by the modified Hummers method. The observed improvements were attributed to the formation of oxygen-containing groups on the surface of the GF which increased the surface hydrophilicity, thereby increasing the absorbed water, and further, enhancing the adsorption of vanadium ions and benefiting the electrode reaction. With the hydrophilic –OH groups providing active sites to facilitate the V(IV)/V(V) redox reaction, the efficiencies of the VRFB employing GF treated by the modified Hummers method was significantly enhanced.

Figure 6

To evaluate electrode performance, charge–discharge testing is most commonly used. Wu et al. [115] also conducted charge–discharge testing of a VRFB cell. Figure 7 displays the charge–discharge curves of two cells with GFs treated by thermal treatment (referred to as cell A) and a modified Hummers method (referred to as cell B). Cell B revealed low charge and high discharge voltage plateaus and could, therefore, achieve high VE because of the increased hydrophilic –OH groups on the GF surface. For the same reason, the cell B exhibited high charge and discharge capacities.

Figure 7

Electrochemical techniques such as those discussed here have shown to be beneficial in understanding the mechanisms that promote both redox reaction activity as well as electrode degradation. What is lacking in the research community, however, are standardized methods of evaluation to enable comparative results. Wu et al. [116] aimed to fill this gap by refining a three-electrode system in terms of GF area and thickness, and working electrode material and relative position to the counter electrode. Their work revealed that optimizing material and parameter selection could not only reduce the influence from side reactions but also ensure reliable results are attained.

2.3.3.2 Physical tools

This section covers the features of physical methods for VRFB electrode diagnosis. Various techniques have been employed, including mass spectroscopy, SEM and transmission electron microscopy (TEM) imaging, atomic force microscopy (AFM), XPS, and 3D tomography.

Mass spectroscopy has the ability to identify species, and therefore, detect side reactions occurring at the electrode. Liu et al. [114] studied graphite corrosion using online mass spectroscopy to monitor gas evolution. Their measurements indicated that, at 1.6 V or higher, CO_2 and CO simultaneously evolved on the graphite electrode; O_2 evolution did not occur until at least 1.8 V. Of the three corrosion gases, O_2 evolved at the fastest rate, followed by CO_2. They also observed that the evolution of CO and CO_2 on the anodic graphite electrode was significantly more severe in a pure 2 M H_2SO_4 environment compared to that in 2 M H_2SO_4 / 2 M $VOSO_4$. It was concluded

that the oxidation of V(IV) to V(V) on the graphite electrode impeded the carbon oxidation reaction, and thus the high concentration of the V(IV) electrolyte was favorable for hindering the electrochemical corrosion of the graphite anode.

The morphology and the crystalline structure of the electrode nanoparticles, which directly affect the transport of electroactive species, can be studied using SEM and TEM imaging, 3D X-ray tomography, and AFM. Liu et al. [114] also presented SEM images of graphite electrodes oxidized at 1.9 V in 2 M H_2SO_4 and 2 M H_2SO_4 / 2 M $VOSO_4$ solutions. Results showed that, in the presence of $VOSO_4$, the oxidized electrode surface is much smoother than that in the absence of $VOSO_4$. This provided further evidence that the presence of V(IV) could reduce graphite corrosion. Also using SEM, the same research group observed inhomogeneous corrosion on the working surface of the electrode which could affect current distribution and electrolyte flow. They also discovered that corrosion was more abundant on the perimeter of the crystallites in the GF [112]. AFM was used in the same study and supplemented the SEM findings by showing that higher potential during anodic polarization resulted in increased active surface area, thereby providing more sites for gas evolution.

Ex-situ XPS has been used to observe variations of the CF surface with respect to changes in the amount of functional groups before and after degradation [111]. The results confirmed that the formation of functional groups on the felt surface is not the main cause for serious changes in the electrical properties of the GF electrodes. XPS has also been used to study overcharged GF. Using XPS, Mohammadi et al. [117] investigated the effect of overcharge on the surface chemistry for three types of GF electrodes. The XPS analysis demonstrated that the overall surface oxygen content of the GFs slightly increased after overcharge; the higher oxidation states allowed for the formation of C–OH, C=O, COOH and COOR functional groups, which are known to catalyze the formation of CO_2 and, therefore, accelerate the electrode corrosion. An increase in carbon-oxygen functional groups was also observed by Liu et al. [112] after anodic polarization at 1.75 V. Further analysis of their XPS data revealed these groups to be in the form of C=O and COOH.

Micro-computed tomography (CT) or 3D tomography is an exceptional diagnostic tool for monitoring the structural changes in GF electrodes during VRFB operation, providing insights into the nano- and micro-structure of the electrodes. Coupling micro-tomography with SEM and XPS measurements, Trogadas et al. [118] were able to reveal the microstructural and chemical evolution within the carbon electrode. The results showed that prolonged operation of the VRFB resulted in extensive microstructural changes in the form of agglomerated fibers. By analyzing the reconstructed 3D images of the cycled electrodes, key geometric parameters of the GF were captured, allowing the calculation of porosity, characteristic tortuosity, and volume specific surface area. Chakrabarti et al. [110] summarized that 3D imaging can quantify surface areas, porosity, and particle sizes and thicknesses, as well as identify different phases, and determine tortuosity and flow configuration of the complex electrode structures. Recently, X-ray computed tomography was used to study the effect of varying compression ratios on CF electrodes [119]. Results showed that the electrode compressed non-linearly and could cause obstructions for the through-plane flow; such an increase in flow resistance may have otherwise been mistakenly associated solely with the decrease in porosity.

Other physical techniques used to evaluate the electrochemical performance of the GF for VRFBs include FTIR and Brunauer-Emmett-Teller (BET) surface area analysis. Li et al. [120] observed via FTIR that electrochemical oxidation decreased the number of C–O groups on the GF surface

while the quantity of –OH and C=O functional groups increased. Specific surface areas of the GF samples were obtained by BET with the finding that an increase of specific area was linked to the electrochemical oxidation treatment.

Although each of these methods can provide significant insight into electrode degradation mechanisms, they do not always represent the full narrative of events and, thus, many challenges still remain. Mass spectroscopy, for example, identifies species by molecular weight and is, therefore, unable to distinguish compounds of identical weights; gas chromatography can help fill this gap. SEM typically provides only qualitative, not quantitative, results; FTIR provides composite, not local, composition details; and BET results have been found to vary with adsorbate gas [121].

2.3.4 Mitigation strategies for electrode degradation

Although the majority of articles published have aimed at enhancing the electrochemical reactivity of CF electrodes, efforts have also been made to mitigate electrode degradation.

2.3.4.1 Voltage and temperature control

The current density at which graphite electrodes begin to corrode greatly depends on both the polarization potential and the operating temperature; in general, the corrosion current density increases with increases to either potential or temperature. As a result, the CE decreases with increased operating temperature and anodic polarization potential. Therefore, one of the strategies to mitigate electrode degradation is to control both the applied potential and operating temperature, thereby preventing gas evolution [112].

Since side reactions usually take place during the charging process, the right cut-off voltage is very important to prevent gas evolution. The cut-off voltage for charging is commonly set to 1.6 V or 1.65 V to prevent parasitic electrode reactions and battery components degradation. Derr et al. [122] investigated the effect of different cut-off voltages on the degradation of CF electrodes in a VRFB. They chose 1.65 V and 1.8 V as the cut-off voltages and compared hydrogen evolution on the negative side and CO_2 evolution on the positive side. For the positive half-cell, they found that CO_2 evolution increased with increasing cut-off voltage; however, the higher cut-off voltage did not increase the evolution of hydrogen on the negative side. In general, the higher cut-off voltage led to a higher rate of degradation. The main reasons for the loss of performance were the imbalance of the electrolyte and the degradation of the CF electrode. By exchanging electrolyte, the electrode degradation was proven to be responsible for 55% and 25% of performance loss for the 1.65 V and the 1.8 V cut-off voltage, respectively.

2.3.4.2 Electrode modification

There are numerous publications investigating the modification of carbon/graphite felt. A variety of modification methods have been reported to improve the electrochemical activity of electrodes, such as nitrogen doping, integration of functional groups, surface modification (e.g., Bi, PbO_2, ZrO_2 etc), and various thermal or other treatments (e.g., ammonium, Fenton's agent, H_2O_2 etc.). These approaches of electrode modification aim to promote electrochemical activities of the electrode. Some publications focus on improving the positive half-cell electrode because the electrochemical kinetic limitations of VRFBs are related to the V(IV)/V(V) reaction while other publications deal with the negative electrode due to the fact that this electrode limits the CE of the battery. In general, most of the reports describe improvement in electrochemical activity of the

electrode. Regarding long-term stability or calendar life, limited research has been conducted; therefore, an opportunity exists to fill this gap in future work.

Shi et al. [123] studied nitrogen-doped graphene as the positive electrode in a VRFB. For the V(IV)/V(V) redox couple reaction, one of their modified electrodes displayed a significant improvement in electrocatalytic activity compared to the unmodified equivalent. Of the four nitrogen species present from the doping process, quaternary-N was the most stable in the acidic environment and, therefore, the most likely contributor of the majority of active sites that resulted in both enhanced activity and overall stability. A similar nitrogen-doping process was more recently applied to GF by Ma et al. [124]. Their modified electrode exhibited extremely strong performance for 800 charge–discharge cycles. Huang et al. [125] demonstrated the preparation of nitrogen- and oxygen-doped CF for VRFB electrodes. Nitrogen and oxygen atoms were introduced into the CF via plasma treatment. The result was enhanced electrocatalytic activity and increased interaction between the CF and electrolyte during cycling. A 13% increase in EE was observed with excellent cycling stability compared to the untreated CF over the 30-cycle test.

Kim et al. [126] prepared a new type of CF with oxygen-rich phosphate groups through direct surface modification with ammonium hexafluorophosphate (NH_4PF_6). The exceptional catalytic properties of the oxygen-rich phosphate groups greatly improved the electrochemical reactivity of the CF towards both V(II)/V(III) and V(IV)/V(V) redox reactions. Undesirable hydrogen evolution was also suppressed by minimizing the redox overpotential in the anolyte. To evaluate the durability of the electrode, short-term cycling tests were conducted. The electrode demonstrated good stability within the VRFB with markedly improved energy efficiency. Estevez et al. [127] introduced tunable oxygen functional groups onto the surface of a GF using O_2 plasma followed by H_2O_2 treatment. Electrode cycling performances of the VRFB with this optimized electrode at different current densities showed no perceived fading after 50 cycles.

Wei et al. [128] developed a GF electrode with a copper nanoparticle deposition for use in VRFBs. It was found that the copper catalyst facilitated a drastic improvement in the electrochemical kinetics of the V(II)/V(III) redox reaction. The VRFB also exhibited excellent stability during the 50 cycles tested. Bismuth nanoparticles have also been reported to have a very positive effect on the performance of a rayon-based GF for the negative electrode of a VRFB [129]. The reversibility of the V(II)/V(III) redox reaction and the long-term half-cell CV cycling performance of the electrode were significantly enhanced. This was explained by the fact that Bi nanoparticles favor the formation of an intermediate compound that reduces V(III) to V(II), thereby proactively competing with the electroreduction of H^+ to form hydrogen. Zhou et al. [130] prepared ZrO_2-modified GF electrodes via immersion-precipitation. In addition to the improved electrochemical activity and reversibility toward the V(IV)/V(V) and V(III) to V(II) redox reactions, the cycle tests demonstrated that the modified electrodes demonstrated exceptional stability with negligible decay after 200 cycles.

In terms of surface treatment, Gao et al. [131] investigated the effect of Fenton's reagent containing H_2O_2 on the GF performance. This modified electrode exhibited excellent electrochemical activity for the V(IV)/V(V) redox reaction and demonstrated higher stability and efficiency than the untreated GF in short-term cycling tests. Through water-activated thermal treatment in a tube furnace, Kabtamu et al. [132] modified GF electrodes. The electrode exhibited high electrochemical activity and reversibility for the V(IV)/V(V) redox reaction, attributed to the abundance of oxygen-containing functional groups produced on the surface of GF fibers as a result

of the water vapor introduced during the treatment. Stability tests showed no observable decay in efficiencies after 30 cycles, indicating that the thermally treated GF was highly stable under strong acidic conditions. More recently, Nia et al. [133] also produced an exceptional amount of oxygen-containing functional groups when they deposited electrochemically reduced graphene oxide on CF electrodes. The modified electrodes exhibited high surface area and conductivity as well as significantly improved capacity retention and EE over 80 cycles.

With respect to electrode modifications to improve performance, the aforementioned methods are mostly to modify raw felts into electrodes with individual unique features. Another possible approach could be a combination with currently recognized and utilized modification methods. For example, GFs can be treated by thermal or chemical methods to create a hydrophilic surface before employing other techniques such as metallic-, graphene-, or polymer-based modifications. Caution should be taken, however, to ensure that the developed modification methods are feasible in the large-scale; factors such as cost, manufacturability, and ease of stack assembly should be considered. Also, regardless of the method, it is important for future researcher to use industry-range vanadium electrolyte concentrations and include long-term cycling as part of their test methods. Of the treatments discussed in this section, only two research groups tested their electrodes beyond 50 cycles. It is well known that surface-modified carbonaceous material initially displays promising performance; however, the modifications and subsequent performance improvements may not be sustainable when prolonged cycling tests are performed.

2.4 Bipolar plates

Bipolar plates are important elements within the VRFB, providing electrical conductivity and physical separation of adjacent cells. As BPs are in direct contact with acidic electrolytes that contain vanadium species in different oxidation states, corrosion of BPs can occur, especially under extended overcharge conditions. Therefore, BP corrosion can be a major issue for the long term stability of VRFBs.

2.4.1 Functionalities and types of bipolar plates

BPs have several functions in a VRFB: (1) physically separating adjacent cells from each other; (2) electrically connecting cells in series, and (3) providing structural support for the stack. Therefore, the main requirements of suitable BPs are high chemical stability in the electrolyte, low electrical resistance and good electrical conductivity, and strong mechanical properties.

As graphite sheets offer higher electrical conductivity, they are conventionally used as the BPs for VRFBs, giving the stack a desirably high power density. However, the graphite plates are costly component of the VRFB stack due to the fabrication of thin graphite plates which are prone to breakage during machining or handling [134]. As a result of the lower cost and superior mechanical properties, a number of VRFB manufacturers have used metal BPs and composite BPs in their low cost stack designs to overcome the problems of graphite BPs. Table 4 summarizes different types of BPs and their advantages and disadvantages, compiled from literature [135]. Carbon composite BPs have had the most attention in recent research with the advantage of lower cost and reduced weight. However, the challenge has been to achieve good conductivity while maintaining mechanical strength.

Table 4

2.4.2 Bipolar plate degradation mechanisms

2.4.2.1 Electrochemical corrosion

Electrochemical corrosion of the BP is mainly caused by the electrical potential between the acidic electrolyte and the BP. According to recent studies, the most important factor affecting the electrochemical corrosion of BPs in VRFB stacks is gas evolution, including H_2, O_2, CO, and CO_2. These gases are induced by the electrical potential in the VRFB stack in the form of side reactions, producing crucial defects on the surface of the BPs or degrading the coating layer of the BPs.

In the positive half-cell, oxidation reactions of carbon, from either the graphite BP or the carbon black filler material in carbon composite BPs, can take place above the critical half-cell voltage of E = 1.6 V [114], particularly when the battery is being overcharged. The oxidation of the graphite or carbon black filler material through side reactions during overcharge is shown in Equations (13-14). These reactions lead not only to the increase in resistance but also to CO_2 formation resulting in delamination and destruction of the composite matrix.

In a VRFB cell, the potential difference is approximately 1.4 V, which may electrolyze water into oxygen and hydrogen (Equations (15-16)) during the VRFB operation. Under certain circumstances, electric current may go through the electrolyte flow path. As a result, a potential difference higher than 1.4 V can be generated on the BP of VRFBs. The newly generated oxygen from electrolysis is very active and easily combines with graphite. Sulfuric acid in the electrolyte is also a very strong oxidizing agent, accelerating the reaction. As for hydrogen evolution, the gas generation rate is particularly severe when metal coating is involved. To increase the corrosion resistance and conductivity, the metal substrate is usually coated with corrosion-resistant metals, such as gold or titanium [136]. However, this coated metal might catalyze the HER in the negative half-cell, competing with the anodic reaction and not only leading to the loss of battery efficiency but also causing bulges and delamination on the surface of BPs during gas evolution.

Electrochemical corrosion of BPs should be investigated based on the types of BPs and the properties of the coating layer. Kim et al. [137] investigated the electrochemical corrosion of composite BPs, on which expanded graphite was coated to decrease the interfacial contact resistance of the carbon composite. They determined that damage to the coating layer of the composite BP during operating could reduce the durability of the composite BP.

Choe et al. [138] investigated the durability of the graphite coating layer on a carbon/epoxy composite BP in VRFB electrolyte with highly concentrated sulfuric acid. Under electrochemical corrosion, they measured the mass loss of graphite with respect to time. Results showed that gas evolution weakened the van der Waals force between the graphene layers, causing electrochemical exfoliation of the graphite. The degradation of the graphite coating then increased the resistance of the BP, thereby decreasing the efficiency of the VRFB. The delaminated graphite was also found to pollute the electrolyte, filling the pores of the CF electrodes, which, in turn, increased the pumping loss.

Liu et al. [139] investigated the corrosion behavior of a carbon–polythene composite BP and the effect of corrosion on its mechanical strength. They observed erosion of the composite BPs due to gas evolution (CO_2, CO, and O_2) when the anodic polarization potential was above 2.0 V in 2 M $VOSO_4$ / 2 M H_2SO_4. The results showed that oxygen functional groups (C=O and O=C–OH) were

formed on the surface of the BPs. Due to the gas evolution, bulges and delamination were also observed on the BP surface, resulting in a decrease in mechanical strength and electro-conductibility of the BPs. Through SEM, it was determined that the conductive porous network within the BPs was also destroyed.

Other factors influencing corrosion include [140]:

- Graphite composition
  - Composition
  - Matrix microstructure
  - Technique adopted for preparing the composite
  - Chemical and physical homogeneity of the BP surface
- Environment
  - Hydrogen-ion concentration (pH) in the solution
  - Specific nature and concentration of other ions in the solution
  - Localized concentration gradients at high SOC
  - Poor fluid distribution that can lead to dead zones and cause high localized overvoltage
  - Cyclic stress and corrosion fatigue

2.4.2.2 Chemical/electroless aging

Up to now, most published papers about BP corrosion have focused on aging due to cycling. In reality, aging not only occurs during battery charge and discharge but also during electroless rest conditions.

Satola et al. [141] studied the influence of SOC on the ex-situ aging of BPs. Graphite-polypropylene BPs were soaked in anolyte and catholyte at 0%, 20%, 80% and 100% SOC for 30, 90, and 190 days. During the immersion, H_2 gas evolution was observed on the surface of BPs in the anolyte. Following immersion, no significant changes in either the surface morphology or the electrical conductivity were detected. However, highly-charged catholyte was found to affect the wettability of BPs. It was theorized that both sulfuric acid and V(V) ions adsorbed in the pores and motivated the oxidation of the graphitic compounds; the exposed surface then allowed for further penetration of water and vanadium ions into the graphite structure. The penetration of V(V) species in the bulk of BPs could be critical for chemical aging, especially when the electric potential difference is increased. To maintain the lifetime of the BPs, storage at a fully charged electrolyte state for prolonged periods of time should be avoided. Nevertheless, further investigation under both operating and rest conditions is needed to fully understand the mechanisms of aging effects of BPs.

2.4.2.3 Oxidation caused by shunt current

There are two types of current flow pathways inside the VRFB stack: the main current path and the shunt current path, as shown in Figure 8 [134]; these can also be referred to as through-plane current pathway and in-plane current pathway, respectively. Along the main current path, electric current flows from cell to cell within the active area of the VRFB stack; this involves passing through the BPs, the CF electrodes, the electrolyte, and the proton exchange membrane. Along the shunt current path, the electric current flows in the direction of the flow channel between cells and is supported by the conductivity of the electrolyte. Shunt currents are not limited to single stacks; they also exist in battery systems consisting of several stacks.

Figure 8

The total resistance, $R_{total,}$ of a unit cell in the main current path can be written as Equation (17) and the total resistance of a unit cell in the shunt current path can be written as in Equation (18) [134]:

$$R_{total} = R_M + 2R_{BP} + 2\frac{1}{\frac{1}{R_{BP/CF}+R_{CF}}+\frac{1}{R_E+R_{E/BP}}} \quad (17)$$

$$R_{shunt} = 2R_{BP} + 2R_{E/BP} + R_E \quad (18)$$

where R_M represents the equivalent resistance of the membrane; R_{BP}, R_{CF}, and R_E represent the resistance of the BP, CF electrode, and electrolyte, respectively. $R_{E/BP}$ represents the interfacial contact resistance between the electrolyte and the BP.

It has been reported that the shunt current might be the driving force behind the corrosion process whereas the main current is less dominant [134]. In the main current flow path, most of the high electrical potential charges exist in the membrane due to the membrane's relatively high resistance in comparison with other cell components; therefore, the main current path does not dominate the electrochemical corrosion of the BP. In the case of the shunt current path, however, the electrical potential between the electrolyte and the BPs is considerably higher. As a result, the shunt current becomes a dominant factor for the electrochemical corrosion of the BP, shortening the life of BPs, affecting the performance of the VRFB, and decreasing the energy transfer efficiency due to an internal self-discharge.

In-plane shunt current can be induced by local potential differences in the VRFB cells. Depending on the concentration of each species in the electrolyte, which is directly related to the SOC, the electrical potential varies from 0 V to 1.6 V based on the Nernst equation. Non-uniform electrolyte flow and non-uniform electrolyte SOC within the VRFB cells may induce electrical potential differences which, in turn, may cause the in-plane electrical current to flow along the BPs. In-plane potential differences can be increased to reach as high as 1.6 V [137].

There are several publications regarding shunt currents, mostly focusing on creating models rather than conducting experimental investigations. Based on the circuit analog method, Xing et al. [142] proposed a stack-level model to investigate shunt current loss within the VRFB. Results showed that the loss due to shunt currents was less than 17% of the total coulomb loss. The stack shunt current of VRFBs was also studied by Yin et al. [14] using both experiments and 3D simulations. They calculated voltages and electrolyte conductivities based on electrochemical distributions and SOC values, and estimated the coulombic loss due to shunt current and vanadium crossover through the membrane. According to their model, the number of cells in the stack played an important role in the loss of shunt currents. Their model could potentially be used to modify the VRFB stack manifold and flow channel designs in an effort to improve system efficiency. Fink et al. [143] compiled a detailed understanding of shunt currents in a VRFB stack and presented shunt current effects for different cell designs and cell counts. They built a stack with an external hydraulic system which allowed them to switch shunt currents on and off. Such control meant that the individual contributions of cross-contamination and shunt currents to the overall self-discharge

could be distinguished; from this, the loss of current could then be calculated by charge conservation measurements. Results showed that an increase in the number of cells in a stack undoubtedly led to an increase in shunt currents.

Shunt currents in a stack are inevitable and are more prevalent with higher cell-count stacks or stacks in series, at high cell voltages, or high SOC. Since these are all conditions found in system applications, it is paramount that the mechanisms relating to shunt currents are investigated thoroughly and well defined so that mitigation efforts can be made. Although models provide a preliminary basis of understanding, more research based on experimental results needs to be conducted.

2.4.3 Diagnostic tools for bipolar plates degradation

2.4.3.1 Property measurements

The performance of BPs greatly depends on the specific type, and therefore the specific properties, of the BP. The degradation mechanisms and degradation rate of BPs are also associated with these properties, including permeability, mechanical properties, and electrical properties.

Composite BPs are usually fabricated by solution casting, during which bubbles or defects could form during the curing process. The reliability of the BP can be verified by measuring permeability; to do so, Nam et al. [144] used a 2-chamber device separated by the BP sample. Air pressure was applied to one chamber and the pressure in the second chamber was observed over time. The gas permeability of the BP could then be calculated. Choe et al. [138] also measured the permeability of various graphite foils via water vapor instead of air. The following standard equation was used to calculate the permeability:

$$Permeability\ coefficient = \frac{WVTR}{P_w} b \quad (19)$$

where WVTR is the water vapor transmission rate, P_w is the pressure difference across the specimen, and b is the thickness of the specimen.

As BPs for VRFBs have to provide strong support to the thin membrane and the CF electrode as well as withstand the high compression pressure of the stack over a long cycle life, BPs must have strong mechanical properties. The mechanical properties of the BP can be measured using a tensile testing machine. The tension tests can observe the elongation and determine the Young's modulus, Poisson's ratio, and tensile strength of the BP.

The resistance of the BP, which affects the ohmic loss in a stack, is an important factor that contributes to the efficiency of VRFBs. The total resistance of a BP can be measured using the four-point probe method in the through-plane. By placing a BP specimen between two CF electrodes, assembling this between two gold-plated copper plates, and applying an electrical current to the testing setup, voltage can then be measured under different compression pressures to calculate the resistance. The areal specific resistance (ASR) of the BP specimen, R_{ASR}, can be calculated by subtracting R_{sub} from R_{total}, shown in Eq. (22). The electrical resistance, R_{total} and R_{sub} are defined in Eqs. (20) and (21), respectively [144].

$$R_{total} = R_{electrode-felt} + R_{felt} + R_{felt-BP} + R_{BP} + R_{felt-BP} + R_{felt} + R_{electrode-felt} \quad (20)$$

$$R_{sub} = R_{electrode-felt} + R_{felt} + R_{electrode-felt} \quad (21)$$

$$R_{ASR} = R_{total} - R_{sub} = R_{BP} + R_{felt} + 2R_{felt-BP} \quad (22)$$

where $R_{electrode\text{-}felt}$ is the interfacial contact resistance between the electrode and the CF, R_{felt} is the bulk resistance of the CF, $R_{felt\text{-}BP}$ is the interfacial contact resistance between the CF and the BP specimen, and R_{BP} is the bulk resistance of the BP specimen. Satola et al. [141] used the same four-point probe method to compare the conductivity of treated and untreated BPs; the results indicated that changes in surface chemistry did not necessarily constitute a change in electrical conductivity.

2.4.3.2 Ex-situ corrosion tests

Kim et al. [134] conducted *ex-situ* tests to investigate the corrosion of graphite-based composite BPs. To best reflect the on-set of corrosion, they mimicked the actual operating conditions of a VRFB. The applied voltage was 1.6 V and the applied current was 20 mA cm^{-2}, approximately 12.5 times higher than the actual shunt currents measured during operation, to accentuate the effects. In their tests, they compared the ASR before and after the tests to observe the corrosion effect. Due to the electrochemical corrosion, the change of ASR as a function of the thickness of the carbon fabric/graphite hybrid composite BPs could clearly be seen; basically, the thicker the coating layer, the greater the increase in ASR.

To investigate the aging of commercially available graphite-polypropylene BPs, Satola et al. [145] conducted corrosion tests in a three-electrode electrochemical cell with catholyte at different SOCs. The applied current density was swept between 100 and -100 mA cm^{-2}. After 3000 cycles in the high SOC catholyte, the BPs show an increase in double layer capacitance, roughness, and open pore volume. The aging effects are ascribed to oxidation and corrosion of the surface. This galvanodynamic aging process intentionally simulates the cycling operation of the VRFB in order to better represent the actual corrosion mechanisms. Mechanical and electrochemical properties such as morphological structure, chemical composition, electrochemical behavior, and electrical conductivity of the BP can be measured using this method.

To measure the stability of their metal-coated and conductive polymer composite BPs in anolyte, Caglar et al. [136] also employed a three-electrode set-up. Potentiodynamic measurements were conducted and, using this method, the research team was able to determine the impact of coating thickness on the BP's electrochemical behavior and hydrogen evolution.

It should be noted that *ex-situ* tests should be, and are often, accompanied with post-mortem physical characterizations such as SEM, TEM, XPS, XRD, FTIR, and X-ray CT in order to obtain the full account of the corrosion mechanisms. As illustrated by these ex-situ tests, there is a variety of methods used in the research community. In order to make true progress in understanding BP degradation mechanisms, an agreement on standardized tests and requirements needs to be established.

2.4.3.3 In-situ corrosion tests

Thus far, the *in-situ* tests for BPs have been conducted only with single cell tests through charge–discharge operation followed by calculation of efficiencies and discharge power density.

Kim et al. [134] studied the durability of their carbon/graphite hybrid BPs by performing five charge–discharge cycles between 1.2-1.6 V at a constant current of 100 mA cm^{-2}, from which the efficiencies were averaged. They found the energy efficiency of the hybrid BP to be 6% higher

than the conventional graphite BP; the low surface hardness of the graphite coating layer on the hybrid BP was thought to be the main contributor to this increased efficiency.

Caglar et al. [136] evaluated the VRFB single cell via galvanostatic charge–discharge tests using metal-coated BPs. The applied constant current varied from 25 to 100 mA cm^{-2} and the obtained voltage was controlled within 0.8 to 1.6 V. They then calculated the discharge power density as well as energy efficiency. Results showed that the ability of their investigated BPs to work at higher current densities was a sign of good electrical conductivity, especially in the through-plane direction. As well, the exceptional discharge power density values indicated advantages to the surface structure for vanadium redox reactions and increased reaction rates.

In-situ corrosion tests for BPs are limited in literature and those results that are published are restricted to very few testing cycles. As with all electrochemical materials in the VRFB, extensive cycling is required to ensure that degradation is fully captured. It is also important to ensure that common electrolyte concentrations are used in order to best simulate an operating VRFB. Finally, cycling tests should be applied in conjunction with *ex-situ* tests, including area specific resistance, as a package of diagnostic tools.

2.4.4 Mitigation strategies for bipolar plate degradation

2.4.4.1 BPs with high corrosion resistance

To ensure long cycle life, recent studies on BPs are still focused on designing BP substrates with good corrosion resistance by either developing novel low cost composite BPs or novel methods to manufacture BPs.

Carbon/epoxy composite BPs are thought to be an ideal substitute for graphite BPs. Lee et al. [146] developed an innovative fabrication process that leaves carbon fibers exposed on the surface of the composite BP, preventing the formation of a resin-rich area. The developed method considerably decreased the ASR of the composite BP without the need for an expanded graphite coating. To reduce the manufacturing cost, Chang et al. [147] designed and fabricated an integrally molded BP; however, real testing in a VRFB was not performed.

To reduce the interfacial resistance of composite BPs, Choe et al. [138] coated composite BPs with pyrolytic graphite and expanded flake-type graphite. It was found that the pyrolytic graphite had higher durability, likely because its graphene sheets were highly oriented in structure due to being crystallized in a planar direction. It was also found that the pyrolytic graphite-coated BPs showed no degradation after 20 h of single cell VRFB testing while the conventional BPs demonstrated partial delamination of graphite, indicating that the newly designed BP was significantly more durable.

Yang et al. [148] proposed a novel design of BPs for VRFBs by injecting molten polyethylene into micropores of the CF. The results showed that the newly designed BPs had higher conductivity, improved mechanical strength, and better overall electrochemical performance and VE compared to that of conventional BPs. These improvements were attributed to the conductive CF network structure attained by the molding method used during fabrication, which affectively lowered the overall resistance of the BP.

2.4.4.2 Other methods

As aforementioned, the electrical potential between the electrolyte and the BP is the main cause of electrochemical corrosion of the BP, furthered by gas evolution induced by that electrical potential. To prevent corrosion, improvements to the uniformity of the BPs in the VRFB stack is essential in order to strictly control the potential applied to all areas of the BP.

For metallic BPs, a metal-doped coating with corrosion-resistance and conductive properties can be applied on the metallic substrate to increase surface homogeneity [136]. As the electrochemical behavior of the coated metal is closely related to the HER, the selection of doping metals with suitable hydrogen evolution overpotential is crucial for the coating layer.

To enhance the electrochemical uniformity and, therefore, durability of carbon composite BPs in VRFBs, Kim et al. [137] developed a method to close the surface cracks on an expanded graphite coating layer by performing compressive tests on the BP. Under compression, permanent transformations to the expanded graphite on the surface can occur to close the micro cracks generated during the fabrication process. SEM observations revealed that the proposed method effectively removed the micro cracks from the surface, thus, efficiently increasing the durability of the carbon composite BPs.

Regardless of which technique is used to improve BP durability and reduce electrochemical corrosion, future research should not just consider laboratory scale results but also take into account the cost and manufacturability of such modifications. Promising small-scale results may not necessarily be feasible in the VRFB market setting.

3 Degradation of VRFB cells

VRFB cell degradation is demonstrated by performance decrease and capacity decay. Aside from the components degradation, VRFB degradation at the cell level is mainly due to imbalanced electrolyte and imbalanced SOC caused by vanadium crossover, water crossover, side reactions at both sides, and V(II) oxidation by air at the anode side.

3.1 Degradation mechanisms at cell level

3.1.1 SOC imbalance

As shown earlier, vanadium species with different oxidation states have different diffusion coefficients and, therefore, their crossover rate from one side of the cell to the other will be different, resulting in one side gaining a higher V concentration while the other side lowers. Luo et al. [149] studied the capacity decay of a VRFB and found that both the imbalanced vanadium active species and asymmetrical valence of vanadium ions in the catholyte and anolyte were the main cause for the decay. Although the same amount of electricity is charged/discharged to/from cathode and anode during the cell operation, in the case of a cation membrane such as Nafion®, the ratio of V(V) over total V in catholyte is not the same as the ratio of V(II) over total V in anolyte. This is attributed to the fact that the total V in the catholyte is different from that in the anolyte. During cycling, the SOC range in the catholyte becomes narrower while in the anolyte it becomes wider. The increased SOC range of the anolyte corresponds to the lower concentration of V(III), resulting in an increase in concentration polarization for the charge process, while the decreased SOC range in catholyte also leads to an increase in concentration polarization for the discharge process.

Imbalanced SOC can also be caused by side reactions at both electrodes. At the anode, the HER may occur and V(II) oxidation by air may lead to the consumption of electricity and active species. At the cathode, oxygen evolution may occur consuming electricity. Wei et al. [150] studied hydrogen evolution in a VRFB using both *ex-situ* (traditional three-electrode cell) and *in-situ* (during VRFB operation) methods. It was found that the HER rate was strongly affected by temperature and that H_2 evolved even at low SOC, contrary to the common belief that the HER occurs at high SOC. Macroscopic observations showed that, at the negative electrode, H_2 bubbles covered the active sites for the V(II)/V(III) redox reaction. At the positive side, O_2 corroded the electrode surface leading to the formation of oxygen-containing functional groups.

3.1.2 Electrolyte imbalance

Ngamasai and Arpornwichanop [151] studied the effect of electrolyte imbalance on the energy capacity of a VRFB. They analyzed the electrolyte imbalance during VRFB operation and calculated the capacity loss at different levels of imbalanced electrolyte. The results showed that the impact of electrolyte imbalance on the capacity and the overall capacity loss could be estimated when the imbalance is detected.

Electrolyte imbalance may be caused by water crossover, which can lead to volume change of the anolyte and catholyte during VRFB operation. However, there are discrepancies regarding water crossover within the literature. Sukkar and Skyllas-Kazacos [90] studied water transfer across different cation membranes with electrolytes at different SOCs during self-discharge. It was found that the SOC affects the water crossover direction and crossover amount. Significant water transfer from the catholyte to the anolyte was found when the VRFB was over-discharged; insignificant water transfer was reported at higher SOCs. Sun et al. [86] observed different volume change patterns with respect to CEMs and AEMs. With Nafion® 115, the volume shifted significantly towards the catholyte in the first several cycles and then volume remained constant. For AEM, the catholyte volume increased and anolyte volume decreased over the first 50 cycles; after 64 cycles, however, the direction of volume change reversed (Figure 9). During cycling, Luo et al. [149] also observed catholyte volume increase and anolyte volume decrease with Nafion® 115. While a significant change in volume was found in the first 5 cycles, slow, continuous volume change was observed in the remaining 195 cycles tested. Wang et al. [152] found that volume change during VRFB cycling never stopped and, after 244 cycles using Nafion® 115 membrane, the anolyte tank became empty. Overall, with CEMs, they concluded that catholyte volume increased and anolyte volume decreased during cycling.

Figure 9

3.2 Mitigation strategies for cell degradation

3.2.1 Mitigation of SOC imbalance

Several methods have been developed to mitigate the SOC imbalance. Whitehead and Harrer [153] developed a method to minimize the SOC imbalance by using the evolved H_2 from the anolyte to reduce V(V) in the catholyte. A single tank with two compartments was used and a carbon paper

coated with catalyst was placed at the catholyte surface. The goal of the catalyst was to catalyze the following reaction:

$$VO_2^+ + 1/2H_2 + H^+ \rightarrow VO^{2+} + H_2O \quad (23)$$

Although this method worked to rebalance the SOC under the conditions used, the effect on an operating VRFB may not be as promising. Only SOC imbalance caused by hydrogen evolution was taken into account; imbalance due to membrane crossover was overlooked due to the lack of continuous cycling. As it known that the SOC range in the catholyte gets narrower when using common cation membranes, reducing charged species will only exacerbate the concentration differential.

The SOC can also be rebalanced by the addition of organic materials to adjust the catholyte average oxidation state. For long term operation, accumulated V(V) during over-charge conditions can be reduced to restore the original average oxidation state. For example, UET applied fructose to rebalance the catholyte oxidation state, restoring the electrolyte energy density [154]. It should be noted, however, that this method was applied to mixed acid electrolyte and, therefore, may not have the same effect on an all-vanadium system.

3.2.2 Electrolyte rebalancing

Remixing is the most commonly used method developed to rebalance the electrolyte. A complete remix, achieved by draining the anolyte and catholyte, mixing them together, and refilling into the tanks, is both time- and labour-consuming. As such, physical partial remix approaches have been developed. Luo et al. [149] performed a physical partial remix by transferring a calculated amount of surplus catholyte back to the anolyte. By applying period partial transfers, longer term cycling with stable capacity was achieved. Rudolph et al. [155] performed a partial remix on a discharged battery, where equal small volumes of both catholyte and anolyte were exchanged. Although this method was successful in balancing the H^+ ions in the half-cells, it did not compensate for the vanadium ion imbalance.

As physical remixing of electrolytes interrupts the VRFB operation, non-interruptive methods have also been developed. Mou et al. [156] invented a method that connected the anolyte and catholyte tanks with a pipe to either periodically or continuously rebalance the electrolyte. This technique allowed the VRFB to operate continuously for a long period of time. The ratio of pipe length and diameter was key to maintain the balance.

After studying the capacity fade for mixed acid electrolyte, UET [154] found that, during long term operation, the ratio of catholyte and anolyte concentration remained constant: 1.3:1. Based on this finding, they designed an overflow system with different volume (volume ratio: 1.3:1) anolyte and catholyte tanks, in which the volume ratio and total vanadium were kept constant. With the new design, the VRFB achieved long term capacity and efficiency stability. However, this design is only valid for the mixed acid electrolyte system. Recently, Wang et al. [152] developed an electrolyte reflow method to solve the electrolyte imbalance issue for the sulfuric acid-vanadium electrolyte system. Figure 10 shows the schematic of their method; without reflow, eventually all of the anolyte will move to the catholyte tank, while with reflow, the anolyte tank will always contain some electrolyte. Similar to the UET method, the volume ratio of catholyte to anolyte is a key parameter affecting the capacity stability and is highly dependent on the operating current density. Cycle life and total capacity were all improved with the reflow method. Shaferner

et al. [157] recently published a dynamic model to simulate the species crossover in a VRFB. They proposed a continuous overflow method to reduce the capacity loss, where the two electrolyte tanks were connected and continuous flow from catholyte to anolyte was allowed during the cycling. The model was validated with experimental measurements and it was found that capacity decay was significantly reduced once an optimal overflow rate was selected. However, electrolyte precipitation was an issue in this method and the reflow could not prevent capacity decay over the long term; complete remixing was needed over long term operation.

Figure 10

Although rebalancing electrolyte by periodical or continuous overflow from one tank to the other has been shown to reduce capacity decay over long term operation, there is a trade-off between reduction of capacity decay and loss of efficiencies. Active species flowing from one side to the other can lead to the consumption of active species in both tanks, which lowers the energy efficiency. Agar et al. [158] observed the loss of efficiencies when they developed a method to reduce capacity decay by using different current at charge and discharge. It was found that capacity loss was reduced when higher current density was used during charge versus discharge. It was also found that the capacity reduction effect was dependent on the membranes used and, for a diffusion-dominated membrane, the capacity loss was less significant than a convection-dominated membrane. However, this technique might be impractical in real applications; in the VRFB industry, constant current operation during change is not typically the method of choice, as SOC is often used to control the charge and discharge. Also high current density operation may lead to lower VE. Currently there are no satisfactory solutions to solve the capacity decay issue without sacrificing efficiencies. Further development on this issue is still needed.

4 Aging prediction

In PEM fuel cells, accelerated stress tests (ASTs) have widely been used as evaluation tools for durability studies in an attempt to significantly reduce the experimental time. In an AST of a PEM fuel cell, different stressors/factors that significantly affect cell performance are applied to the fuel cell to observe degradation of the cell, to identify the probable degradation mechanisms, or to predict the lifetime of the fuel cell [159]. This concept should also apply to the VRFB technology.

4.1 Accelerated stress tests

Unlike the PEM fuel cells, in which ASTs are well established and systematically studied, there are no specific studies on accelerated lifetime testing for VRFBs. Satola et al. [145] have described bulk aging performed on a carbon fiber-polyethylene BP in vanadium electrolyte with 4 M H_2SO_4 at 80 °C for 100 h and on a commercial graphite-epoxy BP by treating it in V(V) electrolyte at 80 °C for 7 days. This is evidence that higher temperature has been used as an acceleration stressor for possible component aging in a real VRFB.

Recently, Mench's group [160] developed a cell-in series (CIS) technique for an accelerated electrode degradation test. In this method, two cells were connected in series with one cell undergoing discharge and the other cell undergoing charge. During the operation, a constant SOC was maintained at a particular charge–discharge condition. Since the CIS method applied extra

stress to the electrodes, it led to faster degradation of the electrode. As expected, electrode performance degradation occurred seven times faster in comparison with typical cycling tests, allowing a swift evaluation of the electrode. They concluded that both aggressively charging and discharging would result in performance loss.

The authors compared the CIS results with those under normal conditions. Figure 11 shows the polarization curves of the cells operated under normal conditions before and after 6 days (54 cycles). It can be seen that, after 54 cycles, slight cell performance degradation was observed. For example, at 100 mA cm^{-2}, the charging potential increased by 5 mV, and discharging potential decreased by 5 mV, indicating some degradation occurred.

Figure 11

After the CIS experiments, however, significant degradation was observed. Figure 12 shows the polarization curves before and after CIS tests. After 6 days of CIS tests, the charging and discharging voltage for the 0.6 V test decreased by more than 100 mV at 100 mA cm^{-2}, a significant degradation compared with normal cycling or even compared with electrodes soaked in 100% SOC solutions. These results indicate that the CIS method is more detrimental to the electrode than normal cycling, and that simply soaking the electrode in V(V) solution is not a stressor for electrode degradation.

Figure 12

The fast degradation in the CIS method might be explained by the increased C=O bonding induced by high SOC. As discussed earlier, oxygen content in the carbon electrode is considered an important factor affecting the VRFB performance. It was previously considered that more O content in the electrode resulted in high VRFB performance [27]. However, more recently Estevez et al. [127] found that only oxygen in O-C=O can enhance VRFB performance, while O-C and O=C are detrimental to the VRFB performance. In the CIS method, XPS analysis shows that SOC is the dominant factor affecting the oxygen content in the positive electrode, thus, causing a fast degradation of the electrode.

4.2 Models for aging prediction

Aging prediction is essential to estimate the overall lifetime and the cost of a battery system. Several models for vanadium redox batteries have been described, however, only one has focused on aging prediction thus far.

Merei et al. [161] presented a multi-physics model which intended to determine all parameters that are essential for aging prediction, including the SOC, the stack and electrolyte temperatures, the corrosion current, and the vanadium concentrations in the reservoirs. This model combines the existing temperature model, electrochemical model, and mechanical model; the temperature model takes into account the temperature changes in the VRFB during charge and discharge, the electrochemical model considers the main electrochemical reactions and side reactions including

H_2 and O_2 evolution and vanadium crossover through the membrane, and the mechanical model scrutinizes the pump losses within the system. Along with these existing models, this multi-physics model also considers the battery's design, electrolyte compositions, voltage, SOC, ambient temperature, and the battery system power. Through simulation, the presented model showed consistency with current experimental results and will become even more accurate once additional hydrogen evolution and corrosion data is available to incorporate into the model.

5 Concluding remarks

VRFBs are considered durable systems with an expected lifetime of over ten years and a cycle life of several thousand cycles; however, degradation mechanisms of the system components have thus far been scattered or scarcely addressed. This review introduced individual components of a VRFB and examined various degradation mechanisms at both cell and component levels. Based on the existing literature, major performance losses can be categorized into degradations of the electrolyte, membrane, electrode, and bipolar plate due to cross-over, side reactions, or other reasons. Following the degradation mechanisms, diagnostic tools to detect degradation mechanisms and applicable mitigation strategies for alleviating degradation were compiled for VRFB components and cells.

In terms of VRFB component degradation, research efforts have greatly focused on electrolyte stability and mitigation via precipitation inhibitors and additives; with the use of spectroscopic tools, precipitation mechanisms are becoming more deeply understood and thus significant advancements have been made that will undoubtedly lead to the desired use of supersaturated electrolyte over an expanded operating temperature range. Membranes for VRFBs have also been widely researched, with numerous formulations developed to improve performance and species crossover; however, membrane degradation in vanadium electrolyte is not well understood and consistency in chemical stability test methods is severely lacking. Carbon-based electrodes and especially bipolar plates have been given considerably less research attention as their degradation is much more complex; on account of the limited studies, therein lies an opportunity to develop standardized test methods to allow for a global coordination of efforts right from the early days of degradation mechanisms investigation. In general, it was found that the experimental techniques used to investigate VRFB electrochemical components varied greatly among research groups, thereby restricting direct comparison of results and limiting united determination of degradation mechanisms.

At this point, the main research trend in the VRFB technology is still to improve its performance and reduce its cost by developing novel materials or optimizing cell design. For example, novel membrane materials are still under development even though low cost perfluorinated membranes with excellent long-term stability are now being commercially manufactured; exploration of low cost electrode materials with high performance and high power density have become one of the hot spots in the development of the technology; and cell architecture/design is being improved to enhance system performance and efficiency.

Compared to performance improvement and cost reduction, degradation of the VRFB system and its components has attracted less attention. Communication with the VRFB industry revealed that degradation of the VRFB system under normal lifetime testing is slow, as the materials used in VRFBs are relatively stable under normal conditions. This indicates that lifetime testing of the VRFB system is extremely time-consuming, which significantly delays the evaluation of novel

materials, not to mention the uptake of the technology itself. Unfortunately, accelerated lifetime testing is not on the agenda and standard protocols and tools for the evaluation of VRFB components are not yet available. The industrial development of prototypes and systems seems to have outpaced the fundamental research. Accelerated lifetime testing and standard VRFB component evaluation protocols and tools are urgently needed. Also, fundamental understanding of the VRFB component and in-depth investigation of the degradation mechanisms are required through combined experimental and computational modeling. We believe that performance degradation of VRFB components, diagnostic tools for VRFB cell/component degradation, and accelerated lifetime testing protocols are the areas that can and should be focused on in the near future.

As for component degradation, different failure modes of material degradation will likely be associated with cell performance loss. To promote longevity, an in-depth investigation that includes all aspects of material selection along with the effects of flowing electrolyte on overall battery performance degradation is needed. Specific areas may include: 1) a detailed evaluation of electrolyte impurity effects on cell performance degradation, 2) further studies to reduce gassing side reactions, 3) component stability at higher potential and long-term cycling, 4) a better understanding of the electrode/electrolyte interface and micro/nano structure on VRFB degradation, and 5) an investigation of more effective mitigation strategies to enhance component stability over a wider operating range.

Throughout the review, we have shed light on VRFB components and their degradation mechanisms, compiled available diagnostic tools, and accumulated mitigation strategies for component and cell degradation, all of which help gain a systematic understanding of VRFB durability and degradation. In particular, future research directions identified within will further guide the development of the technology in finding solutions to existing degradation issues and, ultimately, lead to further technology penetration of the market.

Acknowledgements

This work is financially supported by the National Research Council of Canada's Program of Energy Storage for Grid Security and Modernization.

References

[1]. Weber AZ, Mench MM, Meyers JP, Ross PN, Gostick JT, Liu Q. Redox flow batteries: a review. Journal of Applied Electrochemistry 2011; 41: 1137-1164. DOI: 10.1007/s10800-011-0348-2.

[2]. Skyllas-Kazacos M, Chakrabarti MH, Hajimolana SA, Mjalli FS, Saleem M. Progress in flow battery research and development. Journal of The Electrochemical Society 2011; 158: R55-R79. DOI: 10.1149/1.3599565.

[3]. Bartolozzi M. Development of redox flow batteries. A historical bibliography. Journal of Power Sources 1989; 27: 219-234. DOI: 10.1016/0378-7753(89)80037-0

[4]. Giner J, Swette L, Cahill H. Screening of redox couples and electrode materials. Final report prepared for NASA-Lewis Research Center under Contract Number NAS3-1976; 19760: 1-108.

[5]. Thaller LH. Recent advances in redox flow cell storage systems. Technical Memorandum supported by DOE, DOE/NASA/1 002-79/4, NASA TM-79186 1979; 1-11.

[6]. Ulaganathan M, Aravindan V, Yan Q, Madhavi S, Skyllas-Kazacos M, Lim TM. Recent advancements in all-vanadium redox flow batteries. Advanced Materials Interfaces Article number 1500309 2016; 3: 1-22. DOI: 10.1002/admi.201500309.
[7]. Noack J, Roznyatovskaya N, Herr T, Fischer P. The chemistry of redox-flow batteries. Angewandte Chemie 2015; 127: 9912-9947. DOI: 10.1002/anie.201410823.
[8]. Soloveichik GL. Flow batteries: current status and trends. Chemical Reviews 2015; 115: 11533−11558. DOI: 10.1021/cr500720t.
[9]. Wang W, Luo Q, Li B, Wei X, Li L, Yang Z. Recent progress in redox flow battery research and development. Advanced Functional Materials 2013; 23: 970-986. DOI: 10.1002/adfm.201200694.
[10]. Leung P, Li X, Ponce de León C, Berlouis L, Low CTJ, Walsh FC. Progress in redox flow batteries, remaining challenges and their applications in energy storage. RSC Advances 2012; 2: 10125-10156. DOI: 10.1039/c2ra21342g.
[11]. Alotto P, Guarnieri M, Moro F, Redox flow batteries for the storage of renewable energy: a review. Renewable and Sustainable Energy Reviews 2014; 29: 325-335. DOI: 10.1016/j.rser.2013.08.001.
[12]. Ding C, Zhang H, Li X, Liu T, Xing F. Vanadium flow battery for energy storage: prospects and challenges. Journal of Physical Chemistry Letters 2013; 4: 1281−1294. DOI: 10.1021/jz4001032.
[13]. Blanc C, Rufer A. Chapter 18 Understanding the vanadium redox flow batteries in Paths to Sustainable Energy. Edited by Ng A, Nathwani J. ISBN 978-953-307-401-6, InTechOpen 2010; 333-358, DOI: 10.5772/546.
[14]. Yin C, Guo S, Fang H, Liu J, Li Y, Tang H. Numerical and experimental studies of stack shunt current for vanadium redox flow battery. Applied Energy 2015; 151: 237-248. DOI: 10.1016/j.apenergy.2015.04.080.
[15]. Knehr KW, Kumbur EC. Open circuit voltage of vanadium redox flow batteries: Discrepancy between models and experiments. Electrochemistry Communications 2011; 13: 342-345. DOI: 10.1016/j.elecom.2011.01.020.
[16]. Pavelka M, Wandschneider F, Mazur P. Thermodynamic derivation of open circuit voltage in vanadium redox flow batteries. Journal of Power Sources 2015; 293: 400-408. DOI: 10.1016/j.jpowsour.2015.05.049.
[17]. Shah AA, Al-Fetlawi H, Walsh FC. Dynamic modelling of hydrogen evolution effects in the all-vanadium redox flow battery. Electrochimica Acta 2010; 55: 1125-1139. DOI: 10.1016/j.electacta.2009.10.022.
[18]. Al-Fetlawi H, Shah AA, Walsh FC. Modelling the effects of oxygen evolution in the all-vanadium redox flow battery. Electrochimica Acta 2010; 55: 3192-3205. DOI: 10.1016/j.electacta.2009.12.085.
[19]. Sum E, Skyllas-Kazacos M, A study of the V(II)/V(III) redox couple for redox flow cell applications. Journal of Power Sources 1985; 15: 179-190. DOI: 10.1016/0378-7753(85)80071-9.
[20]. Sum E, Rychcik M, Skyllas-Kazacos M. Investigation of the V(V)/V(IV) system for use in the positive half-cell of a redox battery. Journal of Power Sources 1985; 16: 85-95. DOI: 10.1016/0378-7753(85)80082-3.

[21]. Kear G, Shah AA, Walsh FC. Development of the all-vanadium redox flow battery for energy storage: a review of technological, financial and policy aspects. International Journal of Energy Research 2012; 36: 1105-1120. DOI: 10.1002/er.1863.
[22]. Grande L. Redox flow batteries 2017-2027: markets, trends, applications. https://www.prnewswire.com/news-releases/redox-flow-batteries-2017-2027-markets-trends-applications-300527996.html, accessed on Nov. 26, 2018.
[23]. https://www.engineering.com/DesignerEdge/DesignerEdgeArticles/ArticleID/12312/Massive-800-MegaWatt-hour-Battery-to-Be-Deployed-in-China.aspx, accessed on Nov. 26, 2018.
[24]. Skyllas-Kazakos M, Cao L, Kazakos M, Kausar N, Mousa A. Vanadium electrolyte studies for the vanadium redox battery – a review. ChemSusChem 2016; 9: 1521-1543. DOI: 10.1002/cssc.201600102.
[25]. Cunha Á, Martins J, Rodrigues N, Brito FP. Vanadium redox flow batteries: a technology review. International Journal of Energy Research 2015; 39: 889-918. DOI: 10.1002/er.3260.
[26]. Choi C, Kim S, Kim R, Choi Y, Kim S, Jung HY, Yang JH, Kim HT. A review of vanadium electrolytes for vanadium redox flow batteries. Renewable and Sustainable Energy Reviews 2017; 69: 263-274. DOI: 10.1016/j.rser.2016.11.188.
[27]. Kim KJ, Park MS, Kim YJ, Kim JH, Dou SX, Skyllas-Kazacos M. A technology review of electrodes and reaction mechanisms in vanadium redox flow batteries. Journal of Materials Chemistry A 2015; 3: 16913-16933. DOI: 10.1039/c5ta02613j.
[28]. Schwenzer B, Zhang J, Kim S, Li L, Liu J, Yang Z. Membrane development for vanadium redox flow batteries. ChemSusChem 2011; 4: 1388-1406. DOI: 10.1002/cssc.201100068.
[29]. Doan TNL, Hoang TKA, Chen P. Recent development of polymer membranes as separators for all-vanadium redox flow batteries. RSC Advances 2015; 5: 72805-72815. DOI: 10.1039/c5ra05914c.
[30]. Li X, Zhang H, Mai Z, Zhang H, Vankelecom I. Ion exchange membranes for vanadium redox flow battery (VRB) applications. Energy & Environmental Science 2011; 4: 1147-1160. DOI: 10.1039/c0ee00770f.
[31]. Tokudu N, Kanno T, Hara T, Shigematsu T, Tsutsui Y, Ikeuchi A, Itou T, Kumamoto T. Development of a redox flow battery system. SEI Technical Review 2008; 50: 88-94.
[32]. Skyllas-Kazacos M, Menictas C, Kazacos M. Thermal stability of concentrated V(V) electrolytes in the vanadium redox cell. Journal of The Electrochemical Society 1996; 143: L86-L88. DOI: 10.1149/1.1836609.
[33]. Rahman F, Skyllas-Kazacos M. Solubility of vanadyl sulfate in concentrated sulfuric acid solutions. Journal of Power Sources 1998; 72: 105-110. DOI: 10.1016/S0378-7753(97)02692-X.
[34]. Kazacos M, Cheng M, Skyllas-Kazacos M. Vanadium redox cell electrolyte optimization studies. Journal of Applied Electrochemistry 1990; 20: 463-467. DOI: 10.1007/BF01076057.
[35]. Rahman F, Skyllas-Kazacos M. Vanadium redox battery: Positive half-cell electrolyte studies. Journal of Power Sources 2009; 189: 1212-1219. DOI: 10.1016/j.jpowsour.2008.12.113.

[36]. Kazakos M, Skyllas-Kazacos M. High energy density vanadium electrolyte solutions, methods of preparation thereof an all-vanadium redox cells and batteries containing high energy vanadium electrolyte solutions. WO9635239A1, 1996.
[37]. Kausar N, Howe R, Skyllas-Kazacos M. Raman spectroscopy studies of concentrated vanadium redox battery positive electrolytes. Journal of Applied Electrochemistry 2001; 31: 1327-1332. DOI: 10.1023/A:1013870624722.
[38]. Skyllas-Kazacos M, Peng C, Cheng M. Evaluation of precipitation inhibitors for supersaturated vanadyl electrolytes for the vanadium redox flow battery. Electrochemical and Solid-State Letters 1999; 2: 121-122. DOI: 10.1149/1.1390754.
[39]. Vijayakumar M, Li L, Graff G, Liu J, Zhang H, Yang Z, Hu JZ. Towards understanding the poor thermal stability of V^{5+} electrolyte solution in vanadium redox flow batteries. Journal of Power Sources 2011; 196: 3669-3672. DOI: 10.1016/j.jpowsour.2010.11.126.
[40]. Zhao JX, Wu ZH, Xi JY, Qiu XP. Solubility rules of negative electrolyte $V_2(SO_4)_3$ of vanadium redox flow battery. Journal of Inorganic Materials 2012; 27: 469-474. DOI: 10.3724/SP.J.1077.2012.00469.
[41]. Xiao S, Yu L, Wu L, Liu L, Qiu X, Xi J. Broad temperature adaptability of vanadium redox flow battery – Part 1: electrolyte research. Electrochimica Acta 2016; 187: 525-534. DOI: 10.1016/j.electacta.2015.11.062.
[42]. Cao L, Skyllas-Kazacos M, Menictas C, Noack J. A review of electrolyte additives and impurities in vanadium redox flow batteries. Journal of Energy Chemistry 2018; 27: 1269-1291. DOI: 10.1016/j.jechem.2018.04.007.
[43]. Kubata M, Nakaishi H, Tokuda N. Electrolyte for redox flow battery, and redox flow battery. US7258947B2, 2007.
[44]. Burch AW. Impurity effects in all-vanadium redox flow batteries. Master's Thesis, University of Tennessee, 2015.
[45]. Park JH, Park JJ, Lee HJ, Min BS, Yang JH. Influence of metal impurities or additives in the electrolyte of a vanadium redox flow battery. Journal of The Electrochemical Society 2018; 165: A1263-A1268. DOI: 10.1149/2.0491807jes.
[46]. Kausar N. Studies of V(IV) and V(V) species in vanadium cell electrolyte. PhD Thesis, University of New South Wales, Australia. 2002; http://unsworks.unsw.edu.au/fapi/datastream/unsworks:36347/SOURCE01?view=true, accessed on Nov. 27, 2018.
[47]. Kazacos M. Electrolyte optimization and electrode material evaluation for the vanadium redox battery. MSc Thesis, University of New South Wales, Australia 1989. http://unsworks.unsw.edu.au/fapi/datastream/unsworks:40475/SOURCE01?view=true, accessed on Nov. 27, 2018.
[48]. Mousa A. Chemical and electrochemical studies of V(III) and V(II) solutions in sulfuric acid solution for vanadium battery applications. PhD Thesis, University of New South Wales, Australia, 2003; http://unsworks.unsw.edu.au/fapi/datastream/unsworks:36320/SOURCE01?view=true, accessed on Nov. 27, 2018.
[49]. Li X, Xiong J, Tan A, Qin Y, Liu J, Yan C. Investigation of the use of electrolyte viscosity for online state-of-charge monitoring design in vanadium redox flow battery. Applied Energy 2018; 211: 1050-1059. DOI: 10.1016/j.apenergy.2017.12.009.

[50]. Brooker RP, Bell CJ, Bonville LJ, Kunz HR, Fenton JM. Determining vanadium concentrations using the UV-Vis response method. Journal of The Electrochemical Society 2015; 162: A608-A613. DOI: 10.1149/2.0371504jes.
[51]. Skyllas-Kazacos M, Kazacos M, State of charge monitoring methods for vanadium redox flow battery control. Journal of Power Sources 2011; 196: 8822-8827. DOI: 10.1016/j.jpowsour.2011.06.080.
[52]. Vijayakumar M, Burton SD, Huang C, Li L, Yang Z, Graff GL et al. Nuclear magnetic resonance studies on vanadium(IV) electrolyte solutions for vanadium redox flow battery. Journal of Power Sources 2010; 195: 7709-7717. DOI: 10.1016/j.jpowsour.2010.05.008.
[53]. Griffith WP, Lesniak PJB. Raman studies on species in aqueous solutions Part III. Vanadates, molybdates, and tungstates. Journal of the Chemical Society A 1969; 1066-1071. DOI: 10.1039/J19690001066.
[54]. Griffith WP, Wickins TD. Raman studies on species in aqueous solutions. Part II. Oxy-species of metals of Groups VIA, VA, and IVA. Journal of the Chemical Society A 1967; 675-679. DOI: 10.1039/J19670000675.
[55]. Griffith WP, Wickins TD. Raman studies on species in aqueous solutions Part I. The vanadates. Journal of the Chemical Society A 1966; 1087-1090. DOI: 10.1039/J19660001087.
[56]. Madic C, Begun GM, Hahn RL, Launay JP, Thiessen WE. Raman spectroscopy of neptunyl and plutonyl ions in aqueous solution: Hydrolysis of Np(VI) and Pu(VI) and disproportionation of Pu(V). Inorganic Chemistry 1984; 23: 469-476. DOI: 10.1021/ic00181a025.
[57]. Skyllas-Kazacos M, Kazacos M. Stabilized electrolyte solutions, methods of preparation thereof and redox cells and batteries containing stabilized electrolyte solutions. Pinnacle VRB Ltd., US6143443, 2000; 1-90.
[58]. Mousa A, Skyllas-Kazacos M. Effect of additives on the low temperature stability of vanadium redox flow battery negative half-cell Electrolyte. ChemElectroChem 2015; 2: 1742-1751. DOI: 10.1002/celc.201500233.
[59]. Roe S, Menictas C, Skyllas-Kazacos M. A high energy density vanadium redox flow battery with 3 M vanadium electrolyte. Journal of The Electrochemical Society 2016; 163: A5023-A5028. DOI: 10.1149/2.0041601jes.
[60]. Kausar N, Mousa A, Skyllas-Kazacos M. The effect of additives on the high-temperature stability of the vanadium redox flow battery positive electrolytes. ChemElectroChem 2016; 3: 276-282. DOI: 10.1002/celc.201500453.
[61]. Yeon S-H, So JY, Yun JH, Park S-K, Shin K-H, Jin C-S, Lee YJ. Effect of phosphate additive for thermal stability in a vanadium redox flow battery. Journal of Electrochemical Energy Conversion and Storage 2017; 14: 041007-1-11. DOI: 10.1115/1.4038019.
[62]. Rahman F, Skyllas-Kazacos M. Evaluation of additive formulations to inhibit precipitation of positive electrolyte in vanadium battery. Journal of Power Sources 2017; 340: 139-149. DOI: 10.1016/j.jpowsour.2016.11.071.
[63]. Lee JG, Park SJ, Cho YI, Shul YG. A novel cathodic electrolyte based on $H_2C_2O_4$ for a stable vanadium redox flow battery with high charge–discharge capacities. RSC Advances 2013; 3: 21347-21351. DOI: 10.1039/c3ra44234a.

[64]. Vijayakumar M, Wang W, Nie Z, Sprenkle V, Hu JZ. Elucidating the higher stability of vanadium(V) cations in mixed acid based redox flow battery electrolytes. Journal of Power Sources 2013; 241: 173-177. DOI: 10.1016/j.jpowsour.2013.04.072.
[65]. Oldenburg FJ, Bon M, Perego D, Polino D, Laino T, Gubler L, Schmidt TJ. Revealing the role of phosphoric acid in all-vanadium redox flow batteries with DFT calculations and in situ analysis. Physical Chemistry Chemical Physics 2018; 20: 23664-23673. DOI: 10.1039/c8cp04517h.
[66]. Wang G, Chen J, Wang X, Tian J, Kang H, Zhu X, Zhang Y, Liu X, Wang R. Influence of several additives on stability and electrochemical behavior of V(V) electrolyte for vanadium redox flow battery. Journal of Electroanalytical Chemistry 2013; 709: 31-38. DOI: 10.1016/j.jelechem.2013.09.022.
[67]. Ding C, Ni X, Li X, Xi X, Han X, Bao X, Zhang H. Effects of phosphate additives on the stability of positive electrolytes for vanadium flow batteries. Electrochimica Acta 2015; 164: 307-314. DOI: 10.1016/j.jechem.2018.05.018.
[68]. Prifti H, Parasuraman A, Winardi S, Lim TM, Skyllas-Kazacos M. Membranes for redox flow battery applications. Membranes 2012; 2: 275-306. DOI: 10.3390/membranes2020275.
[69]. Cha SH. Recent development of nanocomposite membranes for vanadium redox flow batteries. Journal of Nanomaterials 2015; Article ID 207525: 1-12. DOI: 10.1155/2015/207525.
[70]. Luo QT, Zhang HM, Chen J, Qian P, Zhai YF. Modification of nafion membrane using interfacial polymerization for vanadium redox flow battery applications. Journal of Membrane Science 2008; 311: 98-103. DOI: 10.1016/j.memsci.2007.11.055.
[71]. Xi J, Wu Z, Teng X, Zhao Y, Chen L, Qiu X. Self-assembled polyelectrolyte multilayer modified nafion membrane with suppressed vanadium ion crossover for vanadium redox flow batteries. Journal of Materials Chemistry 2008; 18: 1232-1238. DOI: 10.1039/b718526j.
[72]. Mai Z, Zhang H, Li X, Xiao S. Nafion/polyvinylidene fluoride blend membranes with improved ion selectivity for vanadium redox flow battery application. Journal of Power Sources 2011; 196: 5737-5741. DOI: 10.1016/j.jpowsour.2011.02.048.
[73]. Fujimoto C, Kim S, Stains R, Wei X, Li L, Yang ZG. Vanadium redox flow battery efficiency and durability studies of sulfonated Diels Alder poly(phenylene)s. Electrochemistry Communications 2012; 20: 48-51. DOI: 10.1016/j.elecom.2012.03.037.
[74]. Choi HS, Oh YH, Ryu CH, Hwang GJ. Characteristics of the all-vanadium redox flow battery using anion exchange membrane. Journal of the Taiwan Institute of Chemical Engineers 2014; 45: 2920-2925. DOI: 10.1016/j.jtice.2014.08.032.
[75]. Kim DH, Park JS, Choun M, Lee J, Kang MS. Pore-filled anion-exchange membranes for electrochemical energy conversion applications. Electrochimica Acta 2016; 222: 212-220. DOI: 10.1016/j.electacta.2016.10.041.
[76]. Lee MS, Kang HG, Jeon JD, Choi YW, Yoon YG. A novel amphoteric ion-exchange membrane prepared by the pore-filling technique for vanadium redox flow batteries. RSC Advances 2016; 6: 63023-63029. DOI: 10.1039/c6ra07790k.
[77]. Wang Y, Wang S, Xiao M, Song S, Han D, Hickner MA, Meng Y. Amphoteric ion exchange membrane synthesized by direct polymerization for vanadium redox flow

battery application. International Journal of Hydrogen Energy 2014; 39: 16123-16131. DOI: 10.1016/j.ijhydene.2014.04.049.

[78]. Hu G, Wang Y, Ma J, Qiu J, Peng J, Li J, Zhai M. A novel amphoteric ion exchange membrane synthesized by radiation-induced grafting α-methylstyrene and N,N-dimethylaminoethyl methacrylate for vanadium redox flow battery application. Journal of Membrane Science 2012; 407-408: 184-192. DOI: 10.1016/j.memsci.2012.03.042.

[79]. Wei X, Li B, Wang W. Porous polymeric composite separators for redox flow batteries. Polymer Reviews 2015; 55: 247-272. DOI: 10.1080/15583724.2015.1011276.

[80]. Tian B, C. Yan W, Wang FH. Proton conducting composite membrane from Daramic/Nafion for vanadium redox flow battery. Journal of Membrane Science 2004; 234: 51-54. DOI: 10.1016/j.memsci.2004.01.012.

[81]. Chieng SC, Kazacos M, Skyllas-Kazacos M. Modification of Daramic, microporous separator, for redox flow battery applications. Journal of Membrane Science 1992; 75: 81-91. DOI: 10.1016/0376-7388(92)80008-8.

[82]. Wei X, Nie Z, Luo Q, Li B, Sprenkle V, Wang W. Polyvinyl chloride/silica nanoporous composite separator for all-vanadium redox flow battery applications. Journal of The Electrochemical Society 2013; 160: A1215-A1218. DOI: 10.1149/2.087308jes.

[83]. Agar E, Knehr KW, Chen D, Hickner MA, Kumbur EC. Species transport mechanisms governing capacity loss in vanadium flow batteries: Comparing Nafion® and sulfonated Radel membranes. Electrochimica Acta 2013; 98: 66-74. DOI: 10.1016/j.electacta.2013.03.030

[84]. Sun C, Chen J, Zhang H, Han X, Luo Q. Investigations on transfer of water and vanadium ions across Nafion membrane in an operating vanadium redox flow battery. Journal of Power Sources 2010; 195: 890-897. DOI: 10.1016/j.jpowsour.2009.08.041.

[85]. Sun J, Shi D, Zhong H, Li X, Zhang H. Investigations on the self-discharge process in vanadium flow battery. Journal of Power Sources 2015; 294: 562-568. DOI: 10.1016/j.jpowsour.2015.06.123.

[86]. Sun J, Li X, Xi X, Lai Q, Liu T, Zhang H. The transfer behavior of different ions across anion and cation exchange membranes under vanadium flow battery medium. Journal of Power Sources 2014; 271: 1-7. DOI: 10.1016/j.jpowsour.2014.07.111.

[87]. Li B, Luo Q, Wei X, Nie Z, Thomsen E, Chen B, Sprenkle V, Wang W. Capacity decay mechanism of microporous separator-based all-vanadium redox flow batteries and its recovery. ChemSusChem 2014; 7: 577-584. DOI: 10.1002/cssc.201300706.

[88]. Skyllas-Kazacos M, Goh L. Modeling of vanadium ion diffusion across the ion exchange membrane in the vanadium redox battery. Journal of Membrane Science 2012; 399-400: 43-48. DOI: 10.1016/j.memsci.2012.01.024.

[89]. Elgammal RA, Tang Z, Sun CN, Lawton J, Zawodzinski Jr. TA. Species uptake and mass transport in membranes for vanadium redox flow batteries. Electrochimica Acta 2017; 237: 1-11. DOI: 10.1016/j.electacta.2017.03.131.

[90]. Sukkar T, Skyllas-Kazacos M. Water transfer behaviour across cation exchange membranes in the vanadium redox battery. Journal of Membrane Science 2003; 222: 235-247. DOI: 10.1016/S0376-7388(03)00309-0.

[91]. Mohammadi T, Chieng SC, Skyllas-Kazacos M. Water transport study across commercial ion exchange membranes in the vanadium redox flow battery. Journal of Membrane Science 1997; 133: 151-159. DOI: 10.1016/S0376-7388(97)00092-6.

[92]. Oh K, Moazzam M, Gwak G, Ju H. Water crossover phenomena in all-vanadium redox flow batteries. Electrochimica Acta 2019; 297: 101-111. DOI: 10.1016/j.electacta.2018.11.151.
[93]. Mohammadi T, Skyllas Kazacos M. Evaluation of the chemical stability of some membranes in vanadium solution. Journal of Applied Electrochemistry 1997; 27: 153-160. DOI: 10.1023/A:1018495722379.
[94]. Sukkar T, Skyllas-Kazacos M. Membrane stability studies for vanadium redox cell applications. Journal of Applied Electrochemistry 2004; 34: 137-145. DOI: 10.1023/B:JACH.0000009931.83368.dc.
[95]. Huang X, Pu Y, Zhou Y, Zhang Y, Zhang H. In-situ and ex-situ degradation of sulfonated polyimide membrane for vanadium redox flow battery application. Journal of Membrane Science2017; 526: 281-292. DOI: 10.1016/j.memsci.2016.09.053.
[96]. Kim S, Tighe TB, Schwenzer B, Yan J, Zhang J, Liu J, Yang Z, Hickner MA. Chemical and mechanical degradation of sulfonated poly(sulfone) membranes in vanadium redox flow batteries. Journal of Applied Electrochemistry 2011; 41: 1201-1213. DOI: 10.1007/s10800-011-0313-0.
[97]. Choi S-W, Kim T-H, Jo S-W, Lee JY, Cha S-H, Hong YT. Hydrocarbon membranes with high selectivity and enhanced stability for vanadium redox flow battery applications: Comparative study with sulfonated poly(ether sulfone)s and sulfonated poly(thioether ether sulfone)s. Electrochimica Acta 2018; 259: 427-439. DOI: 10.1016/j.electacta.2017.10.121.
[98]. Zeng L, Zho TS, Wei L, Jiang HR, Wu MC. Anion exchange membranes for aqueous acid-based redox flow batteries: Current status and challenges. Applied Energy 2019; 233-234: 622-643. DOI: 10.1016/j.apenergy.2018.10.063.
[99]. Heintz A, Wiedemann E, Ziegler J. Ion exchange diffusion in electromembranes and its description using the Maxwell-Stefan formalism. Journal of Membrane Science 1997; 137: 121-132. DOI: 10.1016/S0376-7388(97)00185-3.
[100]. Chieng SC. Membrane processes and membrane modification for redox flow battery applications. PhD thesis, University of New South Wales: Sydney, Australia, 1993.
[101]. Wei W, Zhang H, Li X, Zhang H, Li Y, Vankelecom I. Hydrophobic asymmetric ultrafiltration PVDF membranes: an alternative separator for VFB with excellent stability. Physical Chemistry Chemical Physics 2013; 15: 1766-1771. DOI: 10.1039/c2cp43761a.
[102]. Luo X, Lu Z, Xi J, Wu Z, Zhu W, Chen L, Qiu X. Influences of permeation of vanadium ions through PVDF-g-PSSA membranes on performances of vanadium redox flow batteries. Journal of Physical Chemistry B 2005; 109: 20310-20314. DOI: 10.1021/jp054092w.
[103]. Qiu J, Zhao L, Zhai M, Ni J, Zhou H, Peng J, Li J, Wei G. Pre-irradiation grafting of styrene and maleic anhydride onto PVDF membrane and subsequent sulfonation for application in vanadium redox batteries. Journal of Power Sources 2008; 177: 617-623. DOI: 10.1016/j.jpowsour.2007.11.089.
[104]. Fujimoto C. Advanced membranes for vanadium redox flow batteries (VRFB). DOE Energy Storage Annual Review Meeting, Washington DC, USA, Sept. 26-28, 2016.
[105]. Zhou XL, Zhao TS, An L, Wei L, Zhang C. The use of polybenzimidazole membranes in vanadium redox flow batteries leading to increased coulombic efficiency and cycling

performance. Electrochimica Acta 2015; 153: 492-498. DOI: 10.1016/j.electacta.2014.11.185.
[106]. Zeng L, Zhao TS, Wei L, Zeng YK, Zhang ZH. Highly stable pyridinium-functionalized cross-linked anion exchange membranes for all vanadium redox flow batteries. Journal of Power Sources 2016; 331: 452-461. DOI: 10.1016/j.jpowsour.2016.09.065.
[107]. Chen D, Hickner MA, Agar E, Kumbur EC. Optimizing membrane thickness for vanadium redox flow batteries. Journal of Membrane Science 2013; 437: 108-113. DOI: 10.1016/j.memsci.2013.02.007.
[108]. Derr I, Bruns M, Langner J, Fetyan A, Melke J, Roth C. Degradation of all-vanadium redox flow batteries (VRFB) investigated by electrochemical impedance and X-ray photoelectron spectroscopy: Part 2 electrochemical degradation. Journal of Power Sources 2016; 325: 351-359. DOI: 10.1016/j.jpowsour.2016.06.040.
[109]. Derr I. Electrochemical degradation and chemical aging of carbon felt electrodes in all-vanadium redox flow batteries. Doctor thesis, Department of Biology, Chemistry and Pharmacy of Freie Universität Berlin, Berlin, 2017.
[110]. Chakrabarti MH, Brandon NP, Hajimolana SA, Tariq F, Yufit V, Hashim MA, Hussain MA, Low CTJ, Aravin PV. Application of carbon materials in redox flow batteries. Journal of Power Sources 2014; 253: 150-166. DOI: 10.1016/j.jpowsour.2013.12.038.
[111]. Derr I, Przyrembel D, Schweer J, Fetyan A, Langner J, Melke J, Weinelt M, Roth C. Electroless chemical aging of carbon felt electrodes for the all-vanadium redox flow battery (VRFB) investigated by Electrochemical Impedance and X-ray Photoelectron Spectroscopy. Electrochimica Acta 2017; 246: 783-793. DOI: 10.1016/j.electacta.2017.06.050.
[112]. Liu H, Xu Q, Yan C, Qiao Y. Corrosion behavior of a positive graphite electrode in vanadium redox flow battery. Electrochimica Acta 2011; 56: 8783-8790. DOI: 10.1016/j.electacta.2011.07.083.
[113]. Sun CN, Delnick FM, Aaron DS, Papandrew AB, Mench MM, Zawodzinski Jr TA. Resolving losses at the negative electrode in all-vanadium redox flow batteries using electrochemical impedance spectroscopy. Journal of The Electrochemical Society 2014; 161: A981-A988. DOI: 10.1149/2.045406jes.
[114]. Liu H, Xu Q, Yan C. On-line mass spectrometry study of electrochemical corrosion of the graphite electrode for vanadium redox flow battery. Electrochemistry Communications 2013; 28: 58-62. DOI: 10.1016/j.elecom.2012.12.011.
[115]. Wu X, Xu H, Shen Y, Xu P, Lu L, Fu J, Zhao H. Treatment of graphite felt by modified Hummers method for the positive electrode of vanadium redox flow battery. Electrochimica Acta 2014; 138: 264-269. DOI: 10.1016/j.electacta.2014.06.124.
[116]. Wu L, Wang J, Shen Y, Liu L, Xi J. Electrochemical evaluation methods of vanadium flow battery electrodes. Physical Chemistry Chemical Physics 2017; 19: 14708-14717. DOI: 10.1039/c7cp02581e.
[117]. Mohammadi F, Timbrell P, Zhong S, Padeste C, Skyllas-Kazacos M. Overcharge in the vanadium redox battery and changes in electrical resistivity and surface functionality of graphite-felt electrodes. Journal of Power Sources 1994; 52: 61-68. DOI: 10.1016/0378-7753(94)01938-X.

[118]. Trogadas P, Taiwo OO, Tjaden B, Neville TP, Yun S, Parrondo J, Ramani V, Coppens MO, Brett DJL, Shearing PR. X-ray micro-tomography as a diagnostic tool for the electrode degradation in vanadium redox flow batteries. Electrochemistry Communications 2014; 48: 155-159. DOI: 10.1016/j.elecom.2014.09.010.
[119]. Jervis R, Kok MDR, Neville TP, Meyer Q, Brown LD, Iacoviello F, Gostick JT, Brett DJL, Shearing PR. In situ compression and X-ray computed tomography of flow battery electrodes. Journal of Energy Chemistry 2018; 27: 1353-1361. DOI: 10.1016/j.jechem.2018.03.022.
[120]. Li X, Huang K, Liu Q, Tan N, Chen L. Characteristics of graphite felt electrode electrochemically oxidized for vanadium redox battery application. Transactions of Nonferrous Metals Society of China 2007; 17: 195-199. DOI: 10.1016/S1003-6326(07)60071-5.
[121]. Gandomi YA, Arron DS, Houser JR, Daugherty MC, Clement JT, Pezeshki AM, Ertugrul TY, Mosely DP, Mench MM. Critical review – Experimental diagnostics and material characterization techniques used on redox flow batteries. Journal of The Electrochemical Society 2018; 165: A970-A1010. DOI: 10.1149/2.0601805jes.
[122]. Derr I, Fetyan A, Schutjajew K, Roth C. Electrochemical analysis of the performance loss in all vanadium redox flow batteries using different cut-off voltages. Electrochimica Acta 2017; 224: 9-16. DOI: 10.1016/j.electacta.2016.12.043.
[123]. Shi L, Liu S, He Z, Shen J. Nitrogen-Doped Graphene: Effects of nitrogen species on the properties of the vanadium redox flow battery. Electrochimica Acta 2014; 138: 93-100. DOI: 10.1016/j.electacta.2014.06.099.
[124]. Ma Q, Zeng X-X, Zhou C, Deng Q, Wang P-F, Zuo T-T, Zhang X-D, Yin Y-X, Wu X, Chai L-Y, Guo Y-G. Designing high-performance composite electrodes for vanadium redox flow batteries: experimental and computational investigation. Applied Materials and Interfaces 2018; 10: 22381-22388. DOI: 10.1021/acsami.8b04846.
[125]. Huang Y, Deng Q, Wu X, Wang S. N, O Co-doped carbon felt for high-performance all vanadium redox flow battery. International Journal of Hydrogen Energy 2017; 42: 7177-7185. DOI: 10.1016/j.ijhydene.2016.04.004.
[126]. Kim KJ, Lee HS, Kim J, Park MS, Kim JH, Kim YJ, Skyllas-Kazacos M. Superior electrocatalytic activity of a robust carbon-felt electrode with oxygen-rich phosphate groups for all-vanadium redox flow atteries. ChemSusChem 2016; 9: 1329-1338. DOI: 10.1002/cssc.201600106.
[127]. Estevez L, Reed D, Nie Z, Schwarz AM, Nandasiri MI, Kizewski JP, Wang W, Thomsen E, Liu J, Zhang JG, Sprenkle V, Li B. Tunable oxygen functional groups as electrocatalysts on graphite felt surfaces for all-vanadium flow batteries. ChemSusChem 2016; 9: 1455-1461. DOI: 10.1002/cssc.201600198.
[128]. Wei L, Zhao TS, Zeng L, Zhou XL, Zeng YK. Copper nanoparticle-deposited graphite felt electrodes for all vanadium redox flow batteries. Applied Energy 2016; 180: 386-391. DOI: 10.1016/j.apenergy.2016.07.134.
[129]. Suárez DJ, González Z, Blanco C, Granda M, Menéndez R, Santamaría R. Graphite felt modified with bismuth nanoparticles as negative electrode in a vanadium redox flow battery. ChemSusChem 2014; 7: 914-918. DOI: 10.1002/cssc.201301045.

[130]. Zhou H, Shen Y, Xi J, Qiu X, Chen L. ZrO_2-nanoparticle-modified graphite felt: bifunctional effects on vanadium flow batteries. ACS Applied Materials & Interfaces 2016; 8: 15369−15378. DOI: 10.1021/acsami.6b03761.
[131]. Gao C, Wang N, Peng S, Liu S, Lei Y, Liang X, Zeng S, Zi HF. Influence of Fenton's reagent treatment on electrochemical properties of graphite felt for all vanadium redox flow battery. Electrochimica Acta 2013; 88: 193-202. DOI: 10.1016/j.electacta.2012.10.021.
[132]. Kabtamu DM, Chen JY, Chang YC, Wang CH. Water-activated graphite felt as a high-performance electrode for vanadium redox flow batteries. Journal of Power Sources 2017; 341: 270-279. DOI: 10.1016/j.jpowsour.2016.12.004.
[133]. Nia PM, Abouzari-Lotf E, Woi PM, Alias Y, Ting TM, Ahmad A, Che Jusoh NW. Electrodeposited reduced graphene oxide as a highly efficient and low-cost electrocatalyst for vanadium redox flow batteries. Electrochimica Acta 2019; 297: 31-39. DOI: 10.1016//j.electacta.2018.11.109.
[134]. Kim KH, Kim BG, Lee DG. Development of carbon composite bipolar plate for vanadium redox flow battery. Composite Structures 2014; 109: 253-259. DOI: 10.1016/j.compstruct.2013.11.002.
[135]. Hermann A, Chaudhuri T, Spagnol P. Bipolar plates for PEM fuel cells: a review. International Journal of Hydrogen Energy 2005; 30: 1297-1302. DOI: 10.1016/j.ijhydene.2005.04.016.
[136]. Caglar B, Richards J, Fischer P, Tuebke J. Conductive polymer composites and coated metals as alternative bipolar plate materials for all-vanadium redox flow batteries. Advanced Materials Letters 2014; 5: 299-308. DOI: 10.5185/amlett.2014.amwc.1023.
[137]. Kim KH, Choe J, Nam S, Kim BG, Lee DG. Surface crack closing method for the carbon composite bipolar plates of a redox flow battery. Composite Structures 2015; 119: 436-442. DOI: 10.1016/j.compstruct.2014.08.035.
[138]. Choe J, Lim JW, Kim M, Kim J, Lee DG. Durability of graphite coated carbon composite bipolar plates for vanadium redox flow batteries. Composite Structures 2015; 134: 106-113. DOI: 10.1016/j.compstruct.2015.08.030.
[139]. Liu H, Yang L, Xu Q, Yan C. Corrosion behavior of a bipolar plate of carbon–polythene composite in a vanadium redox flow battery. RSC Advances 2015; 5: 5928-5932. DOI: 10.1039/c4ra13697g.
[140]. Komsiyska L, Kwan A, Hammer EM, Lewerenz M, Barragan SAG. Study of graphite based bipolar plate corrosion for vanadium redox flow batteries. Carolina Nunes Kirchner, June 27, 2013 (Next Energy).
[141]. Satola B, Kirchner CN, Komsiyska L, Wittstock G. Chemical stability of graphite-polypropylene bipolar plates for the vanadium redox flow battery at resting state. Journal of The Electrochemical Society 2016; 163: A2318-A2325. DOI: 10.1149/2.0841610jes.
[142]. Xing F, Zhang H, Ma X, Shunt current loss of the vanadium redox flow battery. Journal of Power Sources 2011; 196: 10753-10757. DOI: 10.1016/j.jpowsour.2011.08.033.
[143]. Fink H, Remy M. Shunt currents in vanadium flow batteries: Measurement, modelling and implications for efficiency. Journal of Power Sources 2015; 284: 547-553. DOI: 10.1016/j.jpowsour.2015.03.057.

[144]. Nam S, Lee D, Lee DG, Kim J. Nano carbon/fluoroelastomer composite bipolar plate for a vanadium redox flow battery (VRFB). Composite Structures 2017; 159: 220-227. DOI: 10.1016/j.compstruct.2016.09.063.
[145]. Satola B, Komsiyska L, Wittstock G, Bulk aging of graphite-polypropylene current collectors induced by electrochemical cycling in the positive electrolyte of vanadium redox flow batteries. Journal of The Electrochemical Society 2017; 164: A2566-A2572. DOI: 10.1149/2.1261712jes.
[146]. Lee D, Lim JW, Nam S, Choi I, Lee DG. Method for exposing carbon fibers on composite bipolar plates. Composite Structures 2015; 134: 1-9. DOI: 10.1016/j.compstruct.2015.07.123.
[147]. Chang CH, Chou HW, Hsu NY, Chen YS. Development of integrally molded bipolar plates for all-vanadium redox flow batteries. Energies 2016; 9: 1-10. DOI: 10.3390/en9050350.
[148]. Yang L, Zhou Y, Wang S, Lin Y, Huang T, Yu A. A novel bipolar plate design for vanadium redox flow battery application. International Journal of Electrochemical Science 2017; 12: 7031-7038. DOI: 10.20964/2017.08.71.
[149]. Luo Q, Li L, Wang W, Nie Z, Wei X, Li B, Chen B, Yang Z, Sprenkle V. Capacity decay and remediation of Nafion based all vanadium redox flow batteries. ChemSusChem 2013; 6: 268-274. DOI: 10.1002/cssc.201200730.
[150]. Wei L, Zhao TS, Xu Q, Zhou XL, Zhang ZH. In-situ investigation of hydrogen evolution behavior in vanadium redox flow batteries. Applied Energy 2017; 190: 1112-1118. DOI: 10.1016/j.apenergy.2017.01.039.
[151]. Ngamasai K, Arpornwichanop A. Analysis and measurement of the electrolyte imbalance in a vanadium redox flow battery. Journal of Power Sources 2015; 282: 534-543. DOI: 10.1016/j.jpowsour.2015.01.188.
[152]. Wang K, Liu L, Xi J, Wu Z, Qiu X. Reduction of capacity decay in vanadium flow batteries by an electrolyte-reflow method. Journal of Power Sources 2017; 338: 17-25. DOI: 10.1016/j.jpowsour.2016.11.031.
[153]. Whitehead AH, Harrer M. Investigation of a method to hinder charge imbalance in the vanadium redox flow battery. Journal of Power Sources 2013; 230: 271-276. DOI: 10.1016/j.jpowsour.2012.11.148.
[154]. UniEnergy Technologies. Two unique advantages of the chloride containing new generation VRFB chemistry. IFBF 2016, Karsruhe, Germany, June 6-8, 2016.
[155]. Rudolph S, Schroder U, Baynov IM. On-line controlled state of charge rebalancing in vanadium redox flow battery. Journal of Electroanalytical Chemistry 2013; 703: 29-37. DOI: 10.1016/j.jelechem.2013.05.011.
[156]. Mou L, Huang M, Klassen A, M. Harper AM. Redox flow battery and method for operating the battery continuously in a long period of time. US 2011/0300417 A1, Dec. 8, 2011.
[157]. Schafner K, Becker M, Turek T. Capacity balancing for vanadium redox flow batteries through electrolyte overflow. Journal of Applied Electrochemistry 2018; 48: 639-649. DOI: 10.1007/s10800-018-1187-1.
[158]. Agar E, Benjamin A, Dennison CR, Chen D, Hickner MA, Kumbur EC. Reducing capacity fade in vanadium redox flow batteries by altering charging and discharging

currents. Journal of Power Sources 2014; 246: 767-774. DOI: 10.1016/j.jpowsour.2013.08.023.
[159]. Zhang S, Yuan XZ, Wang H, Mérida W, Zhu H, Shen J, Wu S, Zhang J. A review of accelerated stress tests of MEA durability in PEM fuel cells. International Journal of Hydrogen Energy 2009; 34: 388-404. DOI: 10.1016/j.ijhydene.2008.10.012.
[160]. Pezeshki AM, Sacci RL, Veith GM, Zawodzinski TA, Mench MM. The cell-in-series method: a technique for accelerated electrode degradation in redox flow batteries. Journal of The Electrochemical Society 2016; 163: A5202-A5210. DOI: 10.1149/2.0251601jes.
[161]. Merei G, Adler S, Magnor D, Sauer DU. Multi-physics model for the aging prediction of a vanadium redox flow battery system. Electrochimica Acta 2015; 174: 945-954. DOI: 10.1016/j.electacta.2015.06.046.

Figure and Table captions

Figure 1 Diagrams of (a) a VRFB energy storage system with separated VRFB stack and electrolyte tanks [11] (Reproduced and modified with permission from Elsevier); (b) a VRFB stack with its components [14] (Reproduced and modified with permission from Elsevier)

Figure 2 Diagrams showing different ions across a) Nafion® 115 and b) VX-20 membrane during the charge–discharge process [86] (Reproduced with permission from Elsevier)

Figure 3 SEM image of SPI-H membrane: (a and b) initial surface and cross-section respectively before VRFB test; (c) surface facing the positive electrode after VRFB test; (d) cross-section after VRFB test; (e) surface facing the negative electrode after VRFB test [95] (Reproduced with permission from Elsevier)

Figure 4 Measured complex impedance spectrum of a V(II)/V(III) single layer anode, at 30 °C and flow rate of 1.5 mL min^{-1} [113] (Reproduced and modified with permission from ECS)

Figure 5 Linear sweep voltammograms of graphite electrodes in different concentrations of $VOSO_4$ with 2 M H_2SO_4 at a scan rate of 5 mV s^{-1} [114] (Reproduced with permission from Elsevier)

Figure 6 Cyclic voltammograms of (a) graphite felt treated by thermal treatment (b) graphite felt treated by modified Hummers method in 0.5 M $VOSO_4$ + 3 M H_2SO_4 [115] (Reproduced with permission from Elsevier)

Figure 7 Charge-discharge profiles of cell A (cell employing graphite felt treated by thermal treatment) and cell B (cell employing graphite felt treated by modified Hummers method) at a current density of 50 mA cm^{-2} [115] (Reproduced with permission from Elsevier)

Figure 8 A schematic drawing of the main current path and the shut current path in the VRFB stack [134] (Reproduced with permission from Elsevier)

Figure 9 Change of electrolyte volume in the positive and negative half-cells during cycle process when using Nafion® 115 or VX-20 as membrane [86] (Reproduced with permission from Elsevier)

Figure 10 Schematic representation of the electrolyte-reflow method [152] (Reproduced with permission from Elsevier)

Figure 11 Polarization curves before and after 54 cycles at 200 mA cm^{-2} [160] (Reproduced and modified with permission from ECS)

Figure 12 iR-corrected polarization curves taken after initial build, 3 d, and 6 d: (a) cell-in-series experiment E: potential hold at 0.6 V and at low SOC; (b) cell-in-series experiment F: potential hold at 1.8 V and at high SOC; and (c) soaked in high SOC solution; curve for cell cycled for 6 d shown for reference [160] (Reproduced with permission from ECS)

Figure 1

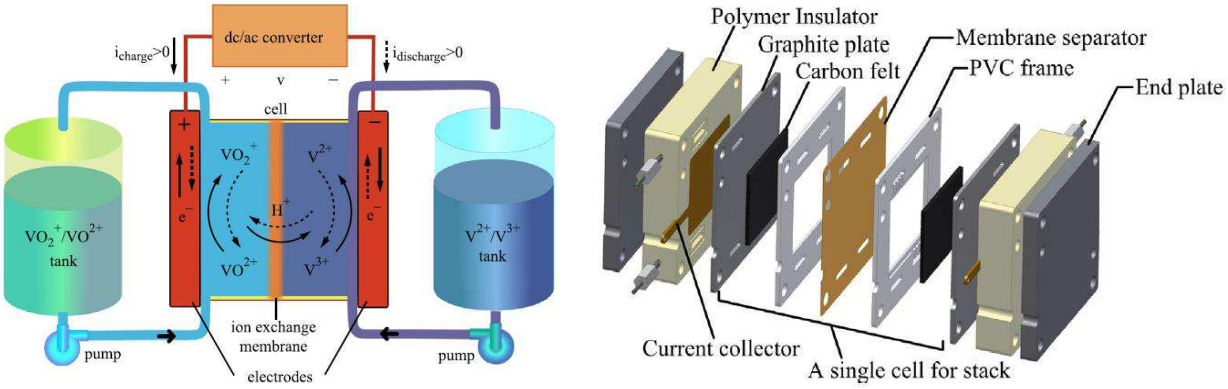

(a) (b)

Figure 2

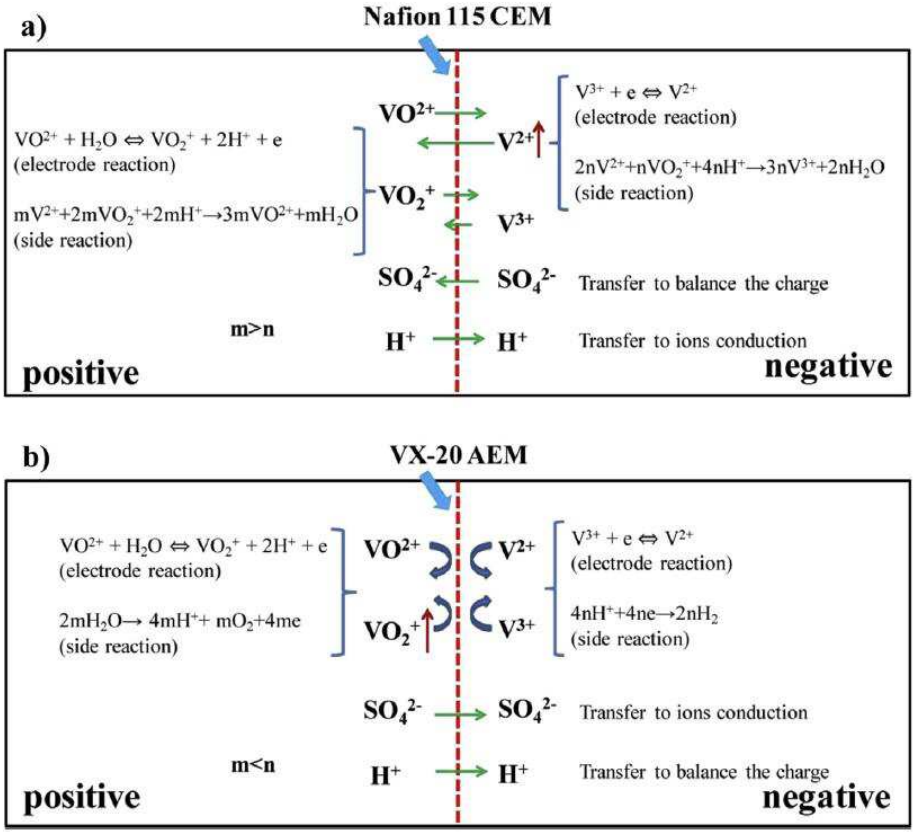

Figure 3

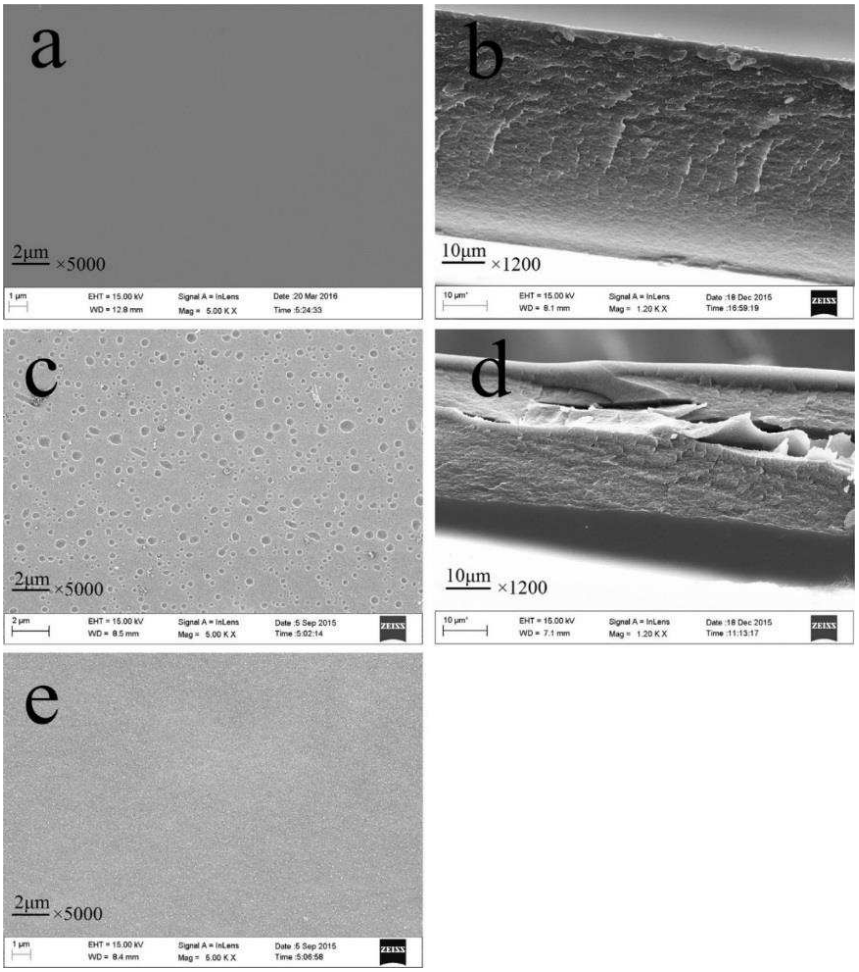

Figure 4

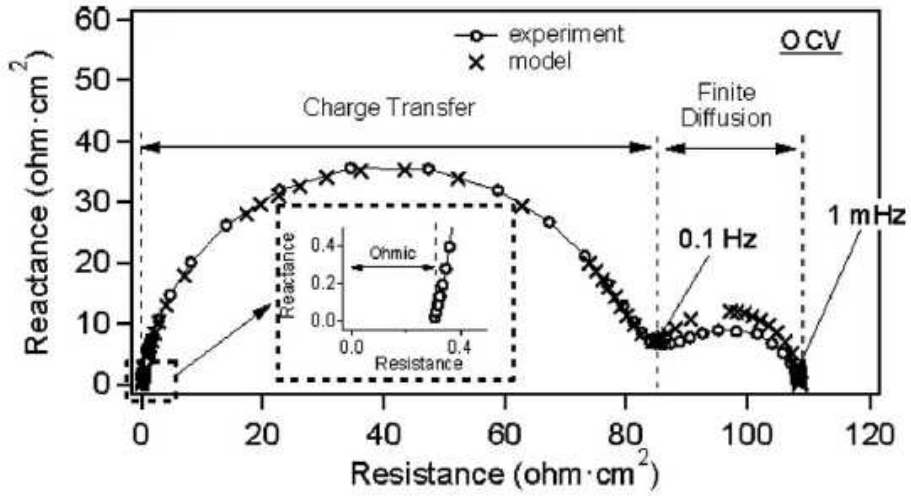

Figure 5

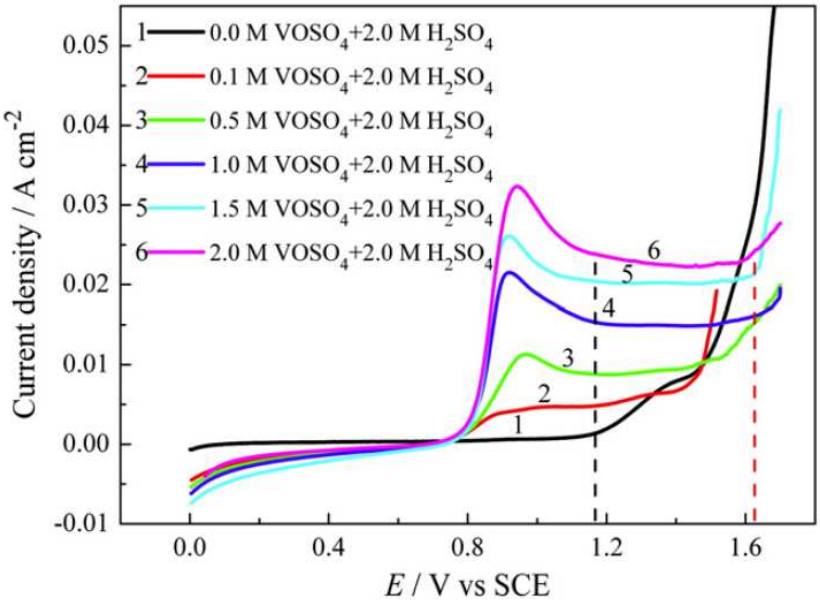

Figure 6

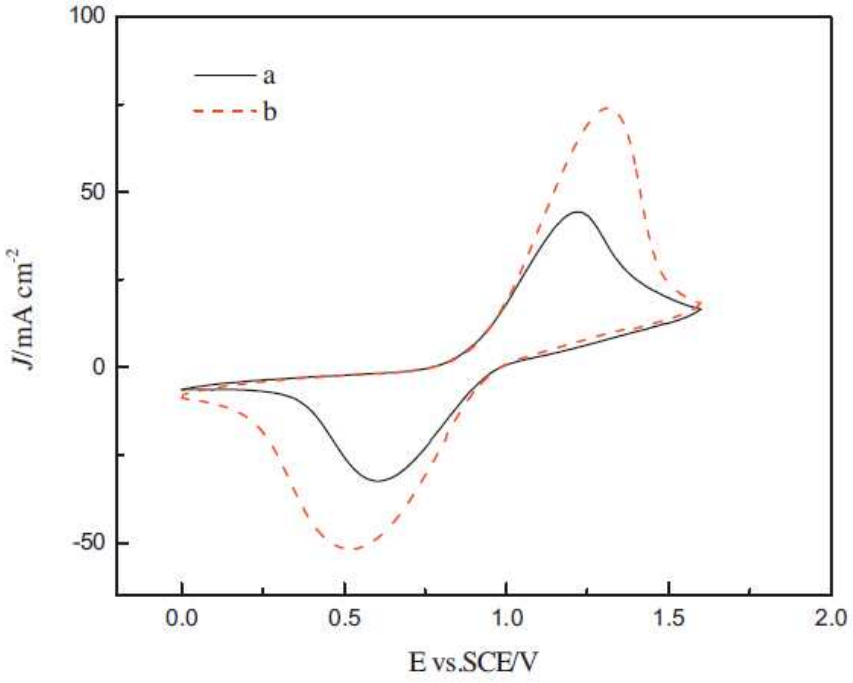

Figure 7

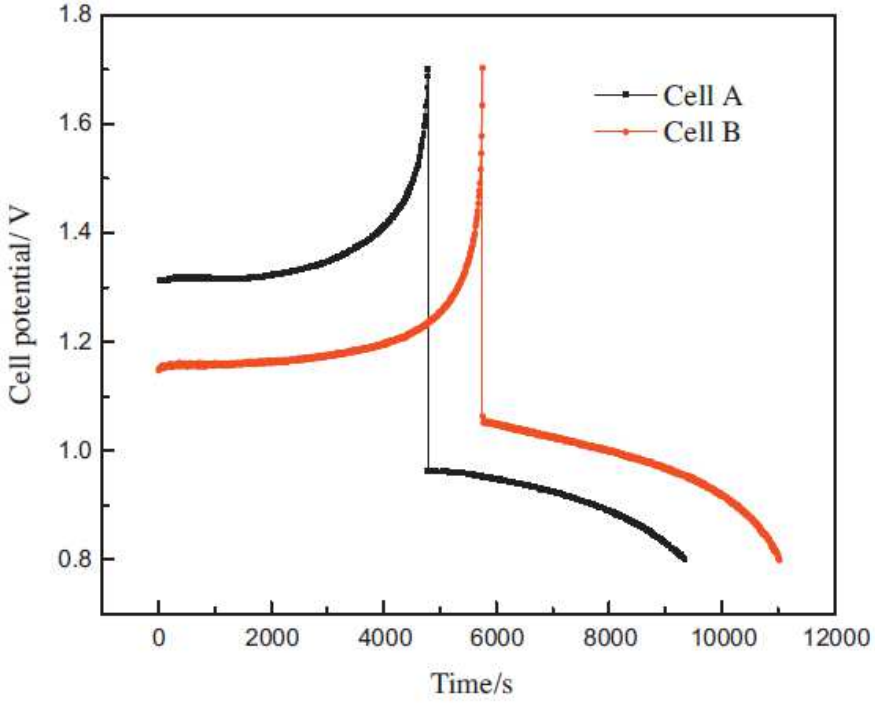

Figure 8

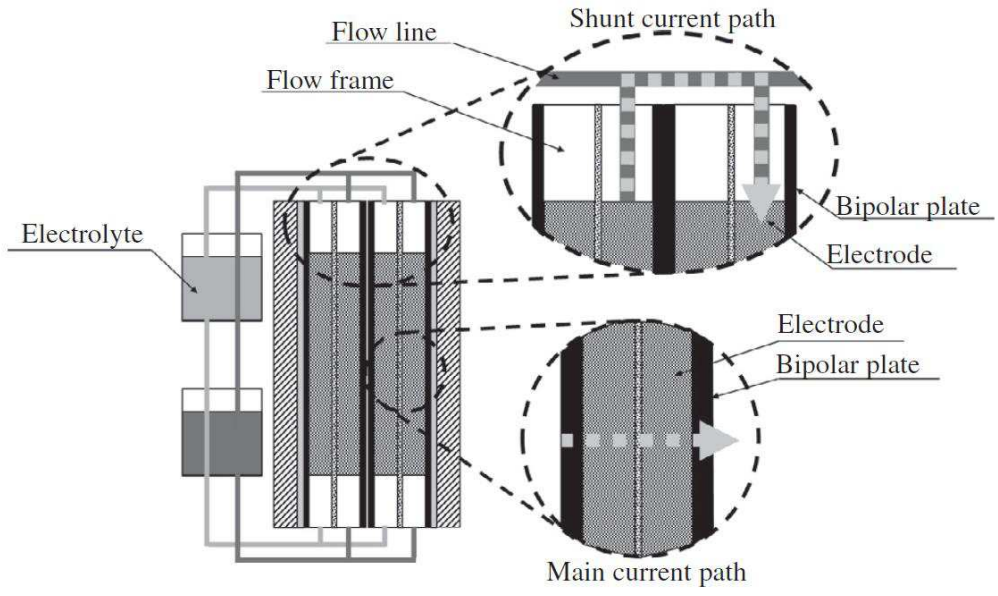

Figure 9

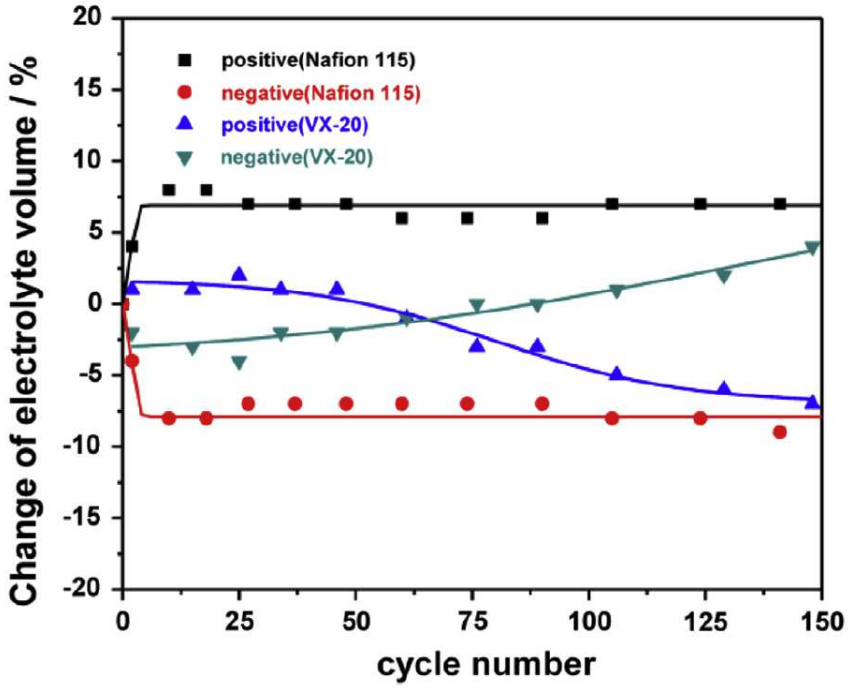

Figure 10

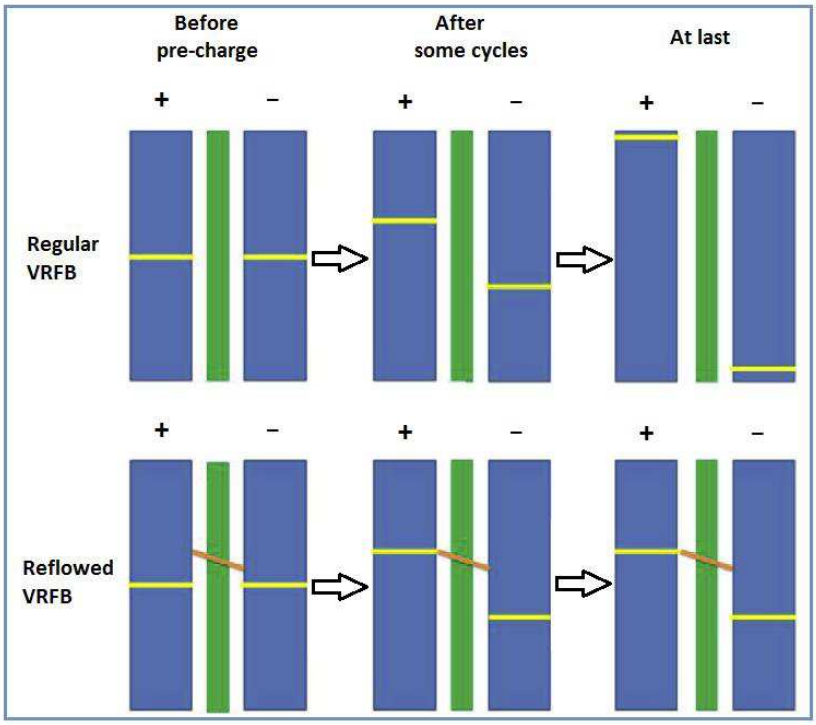

Figure 11

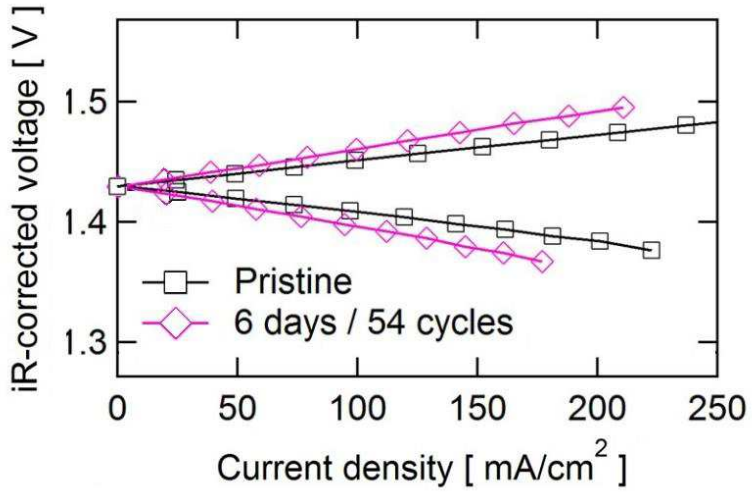

Figure 12

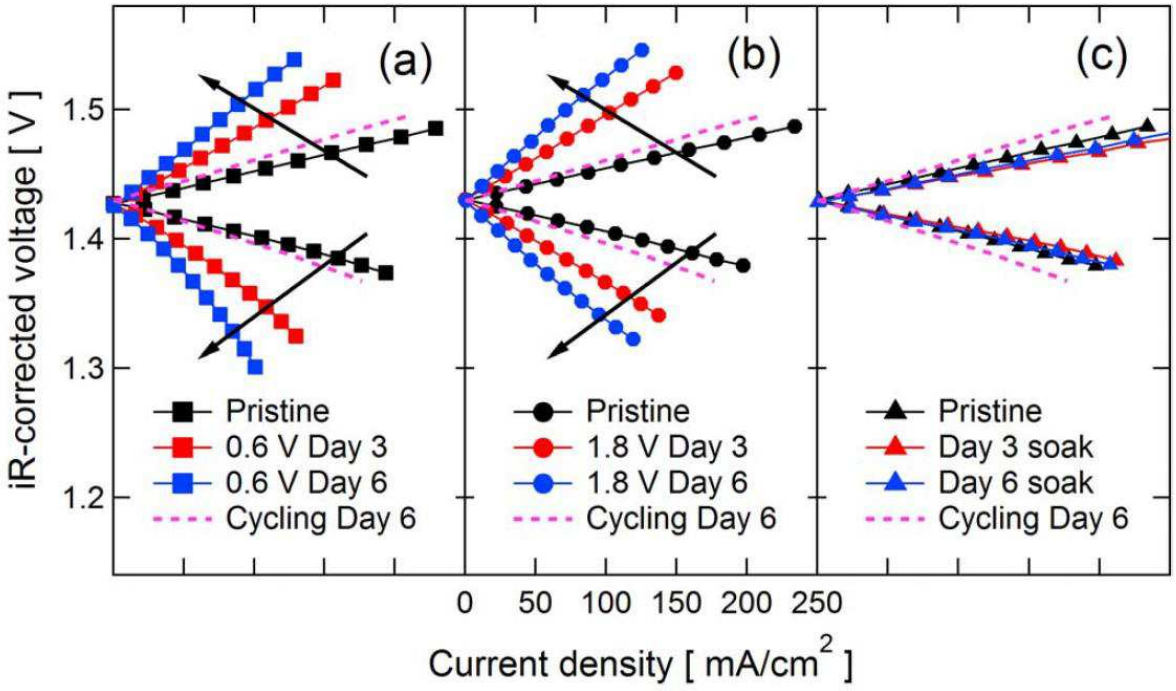

Table 1

Species	Concentration / M	Effect on vanadium reactions
Li^+	0.005	Retarding the kinetics of the V^{2+}/V^{3+} redox reaction
Na^+	-	Negligible effect
K^+	0.05	Decreasing the diffusion rate of V^{3+} ions
Mg^{2+}	-	Negligible effect
Cr^{3+}	0.005	Retarding the kinetics of the V^{2+}/V^{3+} redox reaction and decreasing the diffusion rate of V^{3+} ions
Mn^{2+}	0.02	Decreasing the diffusion rate of V^{3+} ions
Fe^{2+}/Fe^{3+}	0.05	Decreasing the diffusion rate of V^{3+} ions
Co^{2+}	0.05	Decreasing the diffusion rate of V^{3+} ions
Ni^{2+}	0.005	Retarding the kinetics of the V^{2+}/V^{3+} redox reaction and H_2 evolution
Cu^{2+}	0.001	Sedimentation in the negative electrolyte
Zn^{2+}	0.10	Decreasing the diffusion rate of V^{3+} ions
Mo^{6+}	0.001	Sedimentation in both the positive and negative electrolytes

Table 2

Crossover species	Reaction location	Side reaction
V^{2+}	Positive half-cell	$VO^{2+} + V^{2+} + 2H^+ \rightarrow 2V^{3+} + H_2O$
V^{2+}	Positive half-cell	$2VO_2^+ + V^{2+} + 2H^+ \rightarrow 3VO^{2+} + H_2O$
V^{3+}	Positive half-cell	$VO_2^+ + V^{3+} \rightarrow 2VO^{2+}$
VO^{2+}	Negative half-cell	$V^{2+} + VO^{2+} + 2H^+ \rightarrow 2V^{3+} + H_2O$
VO_2^+	Negative half-cell	$2V^{2+} + VO_2^+ + 4H^+ \rightarrow 3V^{3+} + 2H_2O$
VO_2^+	Negative half-cell	$V^{3+} + VO_2^+ \rightarrow 2VO^{2+}$

Table 3

Properties	N115	PVDF	N117	PVDF-g-PSSA	N211	PBI	N212	BrPPO/Py
Reference	[101]	[101]	[102]	[102]	[105]	[105]	[106]	[106]
Thickness (μm)	125	125	180	115	25	30	50	50
Conductivity (mS/cm)	N/A	N/A	58.7	32.2	50.7	15.8	35	23
V(IV) Permeability (10^{-7} cm^2/min)	11.9	7.9	30.0	2.53	18	not detected	7.54	0.25
Current density (mA/cm^2)	80	80	60	60	80	80	100	100
CE (%)	94.5	95.0	89	90	93	99	95.5	97.7
EE (%)	82.0	78.6	67	71	70	65	76.0	77.5
VE (%)	86.8	82.7	75	79	75	65	79.6	79.3
Cycles tested	N/A	1050	N/A	230	20	20	300	530
Capacity decay rate per cycle (%)	N/A	N/A	N/A	0	1.3	0.3	0.067	0.037

Table 4

Type of BP	Advantages	Disadvantages
Graphite BPs	- High conductivity - Low corrosion	- High cost in machining - Vulnerable to breakage
Metal BPs	- High conductivity - Mechanically strong	- Au or Ti coating needed - High cost and low productivity
Carbon composite BPs	- High mechanical strength - Low weight - Low cost	- High electrical contact resistance - Lower conductivity